Västilä, Kaisa; Järvelä, Juha

Characterizing natural riparian vegetation for modeling of flow and suspended sediment transport

Published in:
Journal of Soils and Sediments

DOI:
10.1007/s11368-017-1776-3

Published: 01/10/2018

Document Version
Peer-reviewed accepted author manuscript, also known as Final accepted manuscript or Post-print

Journal of Soils and Sediments

Characterizing natural riparian vegetation for modeling of flow and suspended sediment transport

--Manuscript Draft--

Manuscript Number:	JSSS-D-16-00811R2
Full Title:	Characterizing natural riparian vegetation for modeling of flow and suspended sediment transport
Article Type:	SI: Physical and Ecological Aspects of Mobile Sediments
Section/Category:	Sediments
Corresponding Author:	Kaisa Västilä, D.Sc. (Tech.) Aalto University School of Engineering FINLAND
Corresponding Author Secondary Information:	
Corresponding Author's Institution:	Aalto University School of Engineering
Corresponding Author's Secondary Institution:	
First Author:	Kaisa Västilä, D.Sc. (Tech.)
First Author Secondary Information:	
Order of Authors:	Kaisa Västilä, D.Sc. (Tech.)
	Juha Järvelä, D.Sc. (Tech.)
Order of Authors Secondary Information:	
Funding Information:	Maa- ja vesitekniikan tuki ry (700693) — Not applicable
Abstract:	Purpose: Riparian vegetation imposes a critical control on the transport and deposition of suspended sediment with important implications on water quality and channel maintenance. This paper contributes 1) to hydraulic and morphological modeling by examining the parameterization of natural riparian vegetation (trees, bushes, and grasses) and 2) to the design and management of environmental channels by determining how the properties of natural floodplain plant stands affect the erosion and deposition of suspended sediment. Materials and methods: Laboratory and field data were employed for enhancing physically solid description of the flow-plant-sediment interactions with a view on practical applicability. A drag force parameterization that takes into account the flexibility-induced reconfiguration and the complex structure of foliated plants was validated for small natural trees under laboratory conditions, while the data from a small vegetated compound channel allowed demonstrating the approaches at the field scale. Based on the field data, we identified three key vegetative factors influencing the net deposition and erosion on the floodplain. The significance of these factors was evaluated for vegetative conditions ranging from almost bare soil to sparse willows and dense grasses. Overall, the investigated conditions covered flexible and rigid vegetation with seasonal differences represented by foliated and leafless states. Results and discussion: The drag and reconfiguration of woody plants were reliably predicted under leafless and foliated conditions. Subsequently, we present a new easy-to-use methodology for predicting vegetative drag and flow resistance. The methodology is based on a physically solid parameterization for five widely used coefficients or terms (Eqs. 2-6), with the necessary parameter values presented for common riparian species. The methodology was coupled with existing approaches at the field scale, revealing that increasing vegetation density and the associated decreasing flow velocity within vegetation significantly increased net deposition. Further, deposition increased with increasing cross-sectional vegetative blockage and decreasing distance from the suspended sediment replenishment point. Thus, longitudinal advection was the most important mechanism supplying fine sediment to

	the floodplain, but long continuous plant stands limited deposition. Conclusions: The proposed parameterization (Eqs. 2-6) can be readily implemented into existing hydraulic and morphological models to improve the description of natural vegetation compared to the conventional rigid cylinder representation. The approach is advantageous for evaluating e.g. the effects of both natural succession and management interventions on floodplains. Finally, guidance is provided on how floodplain vegetation can be maintained to manage the erosion and deposition of suspended sediment in environmental channel designs.
Response to Reviewers:	Please, see attachment.

PHYSICAL AND ECOLOGICAL ASPECTS OF MOBILE SEDIMENTS

Characterizing natural riparian vegetation for modeling of flow and suspended sediment transport

Kaisa Västilä[1] • Juha Järvelä[1]

[1]Water Engineering, Aalto University School of Engineering, Espoo, Finland

✉ Kaisa Västilä

kaisa.vastila@aalto.fi

tel. +358 504081390

ORCID: 0000-0002-6034-760X

Abstract

Purpose: Riparian vegetation imposes a critical control on the transport and deposition of suspended sediment with important implications on water quality and channel maintenance. This paper contributes 1) to hydraulic and morphological modeling by examining the parameterization of natural riparian vegetation (trees, bushes, and grasses) and 2) to the design and management of environmental channels by determining how the properties of natural floodplain plant stands affect the erosion and deposition of suspended sediment.

Materials and methods: Laboratory and field data were employed for enhancing physically solid description of the flow–plant–sediment interactions with a view on practical applicability. A drag force parameterization that takes into account the flexibility-induced reconfiguration and the complex structure of foliated plants was validated for small natural trees under laboratory conditions, while the data from a small vegetated compound channel allowed demonstrating the approaches at the field scale. Based on the field data, we identified three key vegetative factors influencing the net deposition and erosion on the floodplain. The significance of these factors was evaluated for vegetative conditions ranging from almost bare soil to sparse willows and dense grasses. Overall, the investigated conditions covered flexible and rigid vegetation with seasonal differences represented by foliated and leafless states.

Results and discussion: The drag and reconfiguration of woody plants were reliably predicted under leafless and foliated conditions. Subsequently, we present a new easy-to-use methodology for predicting vegetative drag and flow resistance. The methodology is based on a physically solid parameterization for five widely used coefficients or terms (Eqs. 2–6), with the necessary parameter values presented for common riparian species. The methodology was coupled with existing approaches at the field scale, revealing that increasing vegetation density and the associated decreasing flow velocity within vegetation significantly increased net deposition. Further, deposition increased with increasing cross-sectional vegetative blockage and decreasing distance from the suspended sediment replenishment point. Thus, longitudinal advection was the most important mechanism supplying fine sediment to the floodplain, but long continuous plant stands limited deposition.

Conclusions: The proposed parameterization (Eqs. 2–6) can be readily implemented into existing hydraulic and morphological models to improve the description of natural vegetation compared to the conventional rigid cylinder representation. The approach is advantageous for evaluating e.g. the effects of both natural succession and management interventions on floodplains. Finally, guidance is provided on how floodplain vegetation can be maintained to manage the erosion and deposition of suspended sediment in environmental channel designs.

Keywords: cohesive sediment, suspended sediment, deposition, vegetation, flow resistance, drag force

1 Introduction

Woody and grassy riparian vegetation growing on river banks and floodplains is a vital part of fluvial ecosystems (e.g. Naiman and Décamps 1997). Accordingly, regulatory norms such as the Water Framework Directive of the European Union demand improving and preserving the diversity, structure and ecological functioning of not only aquatic but also riparian zones. Riparian plant stands can exert a notable control on the seasonal flow resistance and water levels (e.g., Sellin and van Beesten 2004; Västilä et al. 2016) as well as on erosion, deposition and transport processes of fine sediment (e.g. Arboleda et al. 2010; Osterkamp et al. 2012; Gurnell 2014). Predicting these vegetative effects is important e.g. for flood management, agricultural drainage, and stream restoration. Furthermore, suitable maintenance of riparian vegetation can potentially allow for environmentally friendly management of sediment transport. Currently, some of the most severe problems in river systems are related to the excessive, unmanaged transport and deposition of fine sediment (e.g. Owens et al. 2005) with negative effects on fauna and flora (e.g. Wood and Armitage 1997) and water quality through substances sorbed on the sediment (e.g. Uusitalo et al. 2000).

Riparian vegetation is nowadays an essential element in the management of watercourses. For instance, soil bioengineering methods using plant materials (e.g., Li and Eddleman 2002; Studer and Zech 2014) can be combined with conventional technical measures even in highly urbanized or heavily used rivers for stabilizing the banks, protecting against erosion and providing ecological benefits (e.g. Li et al. 2006; Fleischer and Soyeaux 2013). Another application is the excavation or lowering of floodplains as an environmentally preferable alternative to conventional trapezoidal channels for agricultural drainage (e.g., USDA 2007; Västilä and Järvelä 2011) and flood management in low-energy environments (e.g., Sellin and van Beesten 2004; Geerling et al. 2008; Villada Arroyave and Crosato 2010). Such compound (or two-stage) channels are designed to have a narrow cross-section below the floodplain level to ensure that there is no notable net aggradation on the channel bed at low to medium flows, thus bringing sediment transport closer to a state of dynamic equilibrium compared to aggrading over-wide cross-sections (e.g. USDA 2007). Two-stage channels enhance water quality through net retention of suspended sediment (SS), sediment-bound substances and nutrients on the vegetated floodplain (e.g. Mahl et al. 2015; Västilä et al. 2015, 2016). However, the role and characteristics of natural riparian plant stands in controlling erosion, storage or release of sediment are little studied under field conditions (e.g. Osterkamp et al. 2012). Uncertainties associated with the suitable parameterization of natural plants complicate the usage of sophisticated hydraulic and morphological models for real vegetated channels (e.g. Vargas-Luna et al. 2015a).

The modeling of sediment transport rates and morphological processes is sensitive to the parameterization of roughness (e.g., Zinke et al. 2011; Schuurman et al. 2013; Kasvi et al. 2015). In particular, Zinke et al. (2011) state that the correct parameterization of vegetation remains one of the most important factors of uncertainty in morphological modeling. Natural riparian plants are flexible and complex in structure, but they are mostly parameterized as rigid cylinders in hydraulic and morphological models. For shrubs, bushes and trees, the behavior of the woody trunks and branches (herein referred to as stems) under flow is notably different from that of the more flexible foliage (e.g. Vogel 1994; Kouwen and Fathi-Moghadam 2000; Västilä and Järvelä 2014). The flexibility enables the different plant parts to bend and streamline under flow, which is referred to as reconfiguration (e.g. de Langre 2008). As this reconfiguration decreases the drag forces and flow resistance (e.g. Järvelä 2004; Jalonen and Järvelä 2014, Whittaker et al. 2015), the behavior of both foliated and leafless riparian vegetation notably differs from that of rigid elements for which the drag force (F) and flow velocity (u_c) are related as $F \propto u_C^2$ (see also Figures 5 and 6 in Aberle and Järvelä 2013; and Figure 21.4 in Aberle and Järvelä 2015). Overall, the parameterization of natural vegetation in numerical models needs elaboration to take into account the reconfiguration and the complex structure of the plants (e.g. Boothroyd et al. 2015; Solari et al. 2016; Shields et al. 2017).

Additional research is needed on the transport, erosion and deposition rates in flows with natural vegetation (e.g. Vargas-Luna et al. 2015b) since shear-stress based estimates used under unvegetated conditions (e.g. Schuurman et al. 2013; Kasvi et al. 2015) do not necessarily apply to vegetated flows where turbulence is mainly controlled by the vegetative drag (e.g. Nepf 2012). The scarce flume studies that provide sufficient characterization of the investigated natural plants (e.g. Thornton et al. 1997; Ganthy et al. 2015) reveal that the effect of vegetation properties on sediment transport is dampened under conditions of limited sediment supply (Manners et al. 2015). Although settling velocity is the main sediment property controlling deposition (e.g. López and García 1998; Arboleda et a. 2010), vegetation and large woody debris govern local overbank deposition rates and patterns (e.g. Jeffries et al. 2003). Further, vegetative influence on the advective and diffusive supply of suspended sediment SS (e.g. Sharpe and James 1998; Zong and Nepf 2011) generates cross-sectional and reach-scale variability in deposition patterns (e.g. Middelkoop and Asselman 1998; Arboleda et al. 2010). Despite the rich body of literature on floodplain deposition, the investigation by Corenblit et al. (2009) in a gravel-bed river remains one of the few experimental studies examining how various measurable, physically-based properties of natural riparian plant stands explain annual net erosion and deposition rates.

The present paper intends to provide an overview on the characterization of natural riparian plants for flow and suspended sediment transport modeling. For this purpose, data published by the authors and others are revisited for further analyses. The specific objectives are 1) to improve the parameterization of foliated riparian vegetation by considering both the complex plant structures and their reconfiguration, and 2) to determine how the properties of natural floodplain plant stands influence the net erosion and deposition of suspended sediment under real field conditions. Section 2 describes recent developments in modeling vegetative drag and its effects on flow structure, focusing on approaches that can be readily used in practical applications, and Section 3 presents an environmental compound channel where the approaches are applied. Section 4.1 demonstrates the applicability of a recently developed drag force parameterization (Eq. 2) for natural woody vegetation while Section 4.2 shows how the associated methodology can be used in hydraulic and morphological modeling. Sections

4.3–4.4 reveal how the cross-sectional vegetative blockage factor, distance from the sediment supply point, and the flow velocity within the vegetation governed sediment transport at the field site while Section 4.5 provides new knowledge on the management of sediment transport and water quality using vegetated floodplains.

2 Modeling vegetative drag and its influence on flow structure

2.1 Parameterizing the drag of foliated riparian plants

Vegetation can be characterized in hydraulic and morphological models by considering the drag forces (F) exerted by the plants:

$$F = \frac{1}{2}\rho C_D A_C u_C^{2+\chi} \qquad (1)$$

where ρ is the density of the fluid, C_D is the drag coefficient of the object, and A_C is the characteristic reference area of the object. u_C is the characteristic approach velocity, commonly taken as the mean flow velocity in the vegetated layer. The χ exponent was introduced to the velocity term in Equation 1 to be able to describe the non-quadratic relationship between the drag force and flow velocity resulting from the flexibility-induced reconfiguration. In conventional modeling, plants are typically considered to be rigid elements for which χ=0, while natural woody vegetation exhibits values of $\chi = -0.7 \ldots -0.9$ in foliated conditions and $\chi = -0.2 \ldots -0.5$ in leafless conditions at $u_C \leq 1$ m s^{-1} (Jalonen and Järvelä 2014; Västilä and Järvelä 2014; Whittaker et al. 2015).

Based on Eq. 1, several models taking into account the reconfiguration have been presented for estimating the drag and flow resistance of woody vegetation. The models either use bulk parameterizations that lump together the effects of the foliage and stem (e.g. Kouwen and Fathi-Moghadam 2000; Järvelä 2004; Jalonen and Järvelä 2014; Whittaker et al. 2015) or have separate parameterizations for these two differently behaving plant parts (Västilä and Järvelä 2014). In the model of Västilä and Järvelä (2014), the characteristic reference areas are the total frontal projected area of the woody trunk, branches and twigs (A_S) for the stem and the total one-sided leaf area (A_L) for the foliage. The effect of the reconfiguration on the drag is taken into account with reconfiguration terms of the form $(u_C/u_\chi)^\chi$, where u_χ is the reference velocity used for determining the reconfiguration parameter χ (Västilä and Järvelä 2014). u_χ is recommended to be 0.05-0.2 m s^{-1}, i.e. low enough to adequately capture the reconfiguration while high enough to avoid uncertainty associated with the asymptotic nature of the function close to 0 m s^{-1}. The drag forces of reconfiguring woody plants can thus be expressed as

$$F = \frac{1}{2}\rho\left[C_{D\chi,F}\left(\frac{u_C}{u_{\chi,F}}\right)^{\chi_F} A_L + C_{D\chi,S}\left(\frac{u_C}{u_{\chi,S}}\right)^{\chi_S} A_S\right]u_C^{\,2} \qquad (2)$$

where the subscripts F and S denote the parameters determined separately for the foliage and stem, respectively. The drag coefficients $C_{D\chi,F}$ and $C_{D\chi,S}$ have a constant value despite reconfiguration (thus the subscript χ), because the reconfiguration parameters χ_F and χ_S characterize the effect of the reconfiguration on the drag at u_C in relation to the reference velocities $u_{\chi,F}$ and $u_{\chi,S}$. Thus, the values of all the six parameters should be documented (see e.g. Table 2 in Section 4.2). Eq. 2 is dimensionally correct and it is applicable at $u_C \approx 0.05–1.0$ m s^{-1} that are typical flow velocities on floodplains and river banks. The physical factors affecting the parameter values are discussed in detail in Västilä and Järvelä (2014).

We evaluated the performance of Equation 2 for predicting the drag forces of sapling-sized (0.9–3.1 m tall) woody plants (see Section 4.1). This validation included all the available literature data containing the required leaf and stem areas. The data consist of towing tank measurements for nine specimens of *Alnus glutinosa* (Common Alder; Xavier 2009; Dittrich et al. 2012; Jalonen and Järvelä 2014) and three specimens of *Betula pendula* (Silver Birch; Jalonen and Järvelä 2014), for which the reference areas A_L and A_S had been determined. We used the values of χ_F, χ_S, $u_{\chi,F}$, $u_{\chi,S}$, $C_{D\chi,F}$, and $C_{D\chi,S}$ derived by Västilä and Järvelä (2014) from independent data of the corresponding species (summarized in Table 2 in Section 4.2).

Based on Eq. 2 and standard hydraulic theory (see Västilä 2015), we derived a physically solid parameterization for four coefficients or terms that are widely used in hydraulic and morphological modeling and analyses ranging from one-dimensional (1D) considerations to depth-averaged 2D approaches and 3D models (summarized in Table 1). For instance, 3D numerical models typically require representing the vegetation-induced source and sink terms, such as the momentum loss, as the vegetative drag per unit volume (herein referred to as the drag–density parameter C_Da, where a is the vegetative reference area per unit volume). Based on Eq. 2, C_Da can be written for foliated woody vegetation as

$$C_D a = C_{D\chi,F}\left(\frac{u_C}{u_{\chi,F}}\right)^{\chi_F} a_L + C_{D\chi,S}\left(\frac{u_C}{u_{\chi,S}}\right)^{\chi_S} a_S \qquad (3)$$

where a_L and a_S equal $A_L/(A_B z)$ and $A_S/(A_B z)$ where z is the thickness of the examined layer. Further, the drag–area parameter (C_DaH, where H is vegetation height, see e.g. Nepf 2012) that is used to characterize the bulk vegetative drag in depth-averaged models is obtained by integrating Equation 3 over the inundated vegetation height:

$$C_D aH = C_{D\chi,F}\left(\frac{u_C}{u_{\chi,F}}\right)^{\chi_F} \frac{A_L}{A_B} + C_{D\chi,S}\left(\frac{u_C}{u_{\chi,S}}\right)^{\chi_S} \frac{A_S}{A_B} \qquad (4)$$

The vegetative Darcy–Weisbach friction factor (f'') and Manning coefficient (n_{veg}) are used to represent stand- and reach-scale flow resistance and roughness in 1–2D models and computations:

$$f'' = 4\left[C_{D\chi,F}\left(\frac{u_C}{u_{\chi,F}}\right)^{\chi_F}\frac{A_L}{A_B} + C_{D\chi,S}\left(\frac{u_C}{u_{\chi,S}}\right)^{\chi_S}\frac{A_S}{A_B}\right] \tag{5}$$

$$n_{veg} = \frac{Kh^{1/6}}{\sqrt{2g}}\sqrt{C_{D\chi,F}\left(\frac{u_C}{u_{\chi,F}}\right)^{\chi_F}\frac{A_L}{A_B} + C_{D\chi,S}\left(\frac{u_C}{u_{\chi,S}}\right)^{\chi_S}\frac{A_S}{A_B}} \tag{6}$$

The usage of Eqs. 2–6 in flow and sediment transport modeling is discussed in detail in Section 4.2, including the compiled parameter values for common riparian species (Table 2) and a description of the work-flow (Fig. 7).

2.2 Hydraulic description of partly vegetated flows

Approaches for modeling flows where vegetation covers only part of the cross-section mostly have complex descriptions for turbulence at the interfaces between vegetation and open water (e.g. Kang and Choi 2006; Konings et al. 2012). By contrast, the two-layer model of Luhar and Nepf (2013) is straightforward to apply as it describes the momentum balance using coefficients of drag at the interfaces. This two-layer model was originally developed for patchy aquatic vegetation, but a simplified version of the model was found to satisfactorily characterize the reach-scale flow resistance of a vegetated compound channel (Västilä et al. 2016). The two-layer model describes the mean flow velocities in the vegetated parts of the cross-section (u_v) and in the open, unvegetated parts of the cross-section (u_0). The corresponding dimensionless flow velocities (equaling $\sqrt{8/f}$ where f is the Darcy–Weisbach friction factor) are denoted with an asterisk. To be applicable to compound geometry, the model of Luhar and Nepf (2013) can be modified by replacing the channel width by the wetted perimeter (P) and the water depth by the hydraulic radius (R) for the unvegetated and vegetated sections as:

$$u_0^* = \frac{u_0}{(gSR)^{1/2}} = \left[\frac{2P(1-B_X)}{C_f L_b + C_v L_v}\right]^{1/2} \tag{7}$$

$$u_v^* = \frac{u_v}{(gSR)^{1/2}} = \left[\frac{2PB_X + C_v L_v (u_0^*)^2}{C_D aPRB_X}\right]^{1/2} \tag{8}$$

where g is gravitational acceleration and S is energy slope. B_X is cross-sectional vegetative blockage factor that is defined at different water levels as the wetted cross-sectional area covered by vegetation (A_V) divided by the total wetted cross-sectional area A_W (Fig. 1). C_f and C_v are drag coefficients describing the bed shear stress and the shear stress at the interfaces between vegetation and open water, respectively. L_b is the total length of the interface between the bed and open water, i.e., the total wetted perimeter of the unvegetated part of the cross-section (Fig. 1). L_v is the total length of the interface between the vegetation and open water, i.e., the total wetted perimeter along the vegetation interface.

2.3 Effects of vegetation on flow structure and transport processes

The effects of vegetation on the transport of suspended sediment can be evaluated through the advection–diffusion equation (e.g., López and García 1998; Sharpe and James 2006). However, it is not fully established how e.g. the diffusivities of suspended sediment or the erosion and deposition rates depend on the flexibility and density of the plant stands. Since turbulence and transport processes in vegetated flows are related to the vegetative drag (e.g. Nepf 2012), Luhar et al. (2008) describe the tendency of submerged vegetation to cause erosion or deposition by considering the effect of vegetation density on turbulence. Their framework is based on the analysis of the shear layer formed between vegetation and overflow, but a similar shear layer is typically observed at the interface between a vegetated floodplain and an unvegetated main channel (e.g., Kang and Choi 2006).

As summarized by Nepf (2012), for very sparse stands with the drag–area parameter C_DaH<<0.1 (where a is the frontal area of the plants per unit volume and H vegetation height), the vertical profile of the longitudinal mean flow velocity $u_m(z)$ is logarithmic and turbulence is dominated by the vortices generated by the individual stems (pattern 1 in Fig. 2a). Increasing vegetation density results in the formation of an inflection point in the vertical velocity profile at the interface between vegetation and open water, so that turbulence within transitional (~0.1<C_DaH<~0.23) and dense (C_DaH>~0.23) plant stands is mainly generated by the shear-layer vortices (pattern 2 in Fig. 2b) that result from the velocity gradient (Nepf 2012). In sparse and transitional stands, turbulence levels are elevated near the bed, which is hypothesized to cause erosion or re-suspension of sediment (Luhar et al. 2008). In dense stands, the momentum transferred into the stand by the shear-layer vortices is dissipated by the high vegetative drag, and the low values of the flow velocity and near-bed turbulence may allow settling and deposition to take place (Fig. 2b).

The C_DaH limits (Fig. 2) of the approach are mainly based on data from stands of rigid cylinders and have not been validated for describing the effect of vegetation on net erosion or deposition. For natural flexible plant stands, the turbulent flow structure can be predicted e.g. with scaling relations (Sukhodolov and Sukhodolova 2012) or second-order turbulence closures (Ayotte et al. 1999), but this requires reliable estimates of the drag–density parameter (C_Da, Eq. 3) at different mean flow velocities.

3 **Field investigation in a vegetated compound channel**

3.1 Site and monitoring

A three-year field study was conducted at the Ritobäcken Brook (Sipoo, Finland), where a two-stage cross-section was formed by excavating a floodplain at the mean water level in winter 2010 (Fig. 3a). The two-stage approach was selected as an environmentally preferable alternative for improving the conveyance and thus the drainage of the surrounding agricultural fields. Details on the design and construction are reported in Västilä and Järvelä (2011). The floodplain is 850 m long and 4–5 m wide while the main channel is ~2 m wide at bankful conditions. The longitudinal bed slope of the main channel is 0.001–0.002, and the cross-sectional mean velocities range at 0.1–0.3 m s^{-1}. Agricultural fields comprise 13% of the 10 km^2 catchment area while the remainder is mainly forests and mires. The fields, channel bed and channel margins are mainly composed of clay and silt (Västilä and Järvelä 2011; Västilä et al. 2016).

Five 20 m long, differently vegetated sub-reaches were established within a 190 m long test reach in spring 2010 (Västilä and Järvelä 2011). The sub-reaches Grasses-D and -U were sown with pasture grasses, Grasses-N grew naturally established grasses, and Bare-M was intended to have bare soil. Willows-M grew Common Osier (*Salix viminalis*) planted at 0.5 m x 0.5 m spacing. Despite cutting the grassy floodplain and bank vegetation of Willows-M and Bare-M before the seasons when overbank flows occurred, sparse ≤0.05 m high stubble of grass remained in these sub-reaches. Both the low flow channel and the two-stage test reach are fairly straight (e.g. Fig. 4).

Site monitoring, with details reported in Västilä et al. (2016), included repeated cross-sectional surveys in two cross-sections of each sub-reach (Fig. 4) in three consecutive years to determine the annual net deposition. The cross-sectional geometry was measured at 0.2–0.4 m intervals in altogether 200 points with a point gauge, and the accuracy in determining the ground level was ± 6 mm. The fluffy bed prevented obtaining reliable measurements of the vertical changes in the main channel. The water levels of the sub-reaches were recorded at different flows (Fig. 4). Vegetation height was determined for the sub-reaches every spring and autumn while vegetation dry mass and frontal area per unit volume were determined every autumn. To compute the transported loads of suspended sediment, sensors recorded water levels and turbidities at 5-minute intervals at continuous monitoring stations located at the upstream and downstream ends of the 190 m long test reach (Fig. 4). Discharge and suspended sediment concentration were obtained from the sensor readings using site-specific rating curves (Västilä et al. 2016).

Eight water samples were collected at different flow events with suspended sediment concentration of SSC=60–320 mg l^{-1} from the downstream station (Fig. 4). During the sampling, floodplain water depth was ≤0.30 m and relative depth (floodplain water depth divided by the total water depth) ≤0.38. In the laboratory, the samples were subjected to laser-based analyses (LS 13 320 MW by Beckman Coulter) with a 5-min ultrasound pre-treatment. The dispersed suspended sediment had D_{10}=0.48 μm (standard deviation SD=0.06), D_{50}=2.6 μm (SD=0.6), and D_{90}=11 μm (SD=2.5), with all the particles finer than 33 μm. To give an indication on the cohesion that markedly affects the behavior of SS (e.g. Droppo 2001), suspended sediment was also analyzed in the flocculated form after only gentle mixing. Similar to Thonon et al. (2005), the average effective grain sizes were 2–4 times greater than in the dispersed form: D_{10}=1.3 μm (SD=0.6), D_{50}=7.8 μm (SD=1.1), and D_{90}=39 μm (SD=6), with no relationship to SSC. However, we acknowledge that these effective sizes determined in the laboratory may somewhat differ from the actual *in situ* values. Composite samples of the top 1 cm of the sediment deposited on the middle of the floodplain were collected in the sub-reaches Grasses-U and Bare-M shortly after the monitoring ended. After drying at 105 °C and gentle crushing, the dispersed particle size distribution was analyzed using both the hydrometer method and the laser-based method with a 5-min ultrasound pre-treatment. The organic content was ~10% for the floodplain and bed sediment and 15–43% for the suspended sediment.

Settling velocities (w_s) were estimated for the SS flocs of different sizes using the relationship determined by Thonon et al. (2005) for cohesive suspended flocs of approximately similar size distribution: w_s=2.7×10$^{-7}D^{1.57}$, where D is the floc diameter in µm and w_s has the unit m s^{-1}. The length scales over which SS flocs of different sizes are advected before being deposited (x_a) were computed as $x_a= u_vH/w_s$ (Zong and Nepf 2011) using the estimated w_s, the representative h=0.25 m and the associated u_v=0.027 m s^{-1} (mean value for the grassy sub-reaches obtained as described in Section 3.2). We obtained an estimate of the percentage of SS depletion within long, wide plant stands by dividing the distance to the SS replenishment point by the advection length scale.

3.2 Modeling and analyses

The differences in the vegetation properties and rates of deposition between the excavated bank, inner floodplain, and the ~1.2 m floodplain–main channel interface region are reported by Västilä et al. (2016) whereas the present paper focuses on the relevant physical processes at the reach scale. Thus, the data were spatially averaged at the cross-sectional or sub-reach scale for the present modeling and analyses, assuming Grasses-N to be representative of the areas located outside of the sub-reaches.

The flow velocities and discharges within floodplain vegetation as well as the total discharges on the floodplain were modelled using the approaches presented in Section 2. We firstly computed (Eqs. 7–8) the dimensionless velocities u_0^* and u_v^* using the values of L_b, L_v, P, R, B_X and a available from the cross-sectional and vegetation surveys. The velocities are representative of the summer/autumn conditions as a was analyzed in autumn when overbank flows with high SSC occur (Västilä and Järvelä 2011). We assumed $C_f = C_v$, as supported by Luhar and Nepf (2013), and used $C_f = C_v$ =0.079 according to the calibration of a simplified version of the model to the same site (Västilä et al. 2016). For the *S. viminalis* willows, C_Da was expressed according to Eq. 3, using the a_L and a_S determined through *in-situ* sampling and the χ and $C_{D\chi}$ values obtained for the same species in independent laboratory experiments (Västilä and Järvelä 2014; see Table 2 in Section 4.2). For the grassy vegetation, we determined a as the frontal projected area per unit volume of the grass blades through *in-situ* sampling and used the commonly assumed C_D=1 and χ=0 (e.g. Luhar and Nepf 2013) as the grasses were observed to behave fairly rigidly at the low flow velocities (u_v=0.02−0.06 m s^{-1} for the grassy vegetation, see Section 4.3). Sensitivity analyses were conducted for the grasses using C_D=0.5 and C_D=1.5.

The discharges within the vegetation (Q_v) and in the open part of the cross-section (Q_0) were estimated by multiplying the measured bulk discharge (Q) by the predicted shares of the discharge, Q_v =

$Qu_v^* B_X$ / $[u_v^* B_X + u_0^*(1 - B_X)]$ and $Q_0 = Qu_0^*(1 - B_X)$ / $[u_v^* B_X + u_0^*(1 - B_X)]$, respectively. The flow velocities were derived as $u_v = Q_v/(B_X A_W)$ instead of $u_v = u_v^*(gSR)^{1/2}$ (Eq. 8), because the relative errors were expected to be lower for Q than for the $(gSR)^{1/2}$ term. For emergent vegetation, the discharge on the floodplain (Q_{fp}) equals Q_v while for submerged vegetation Q_{fp} was computed by summing Q_v and the discharge above the vegetation computed from u_0.

The significance of different factors for explaining the mean annual net erosion and deposition on the excavated floodplain and bank was evaluated with multiple regression analysis. Sediment properties were expected to be approximately constant because the sub-reaches were located close to each other (Fig. 4), with 94.5% of the incoming sediment load passing the entire reach without being deposited (see Fig. 11). Thus, the particle settling velocities and bulk sediment loads were assumed to be similar in all sub-reaches and were not directly included in the statistical analysis. Based on the observations of Västilä et al. (2016), the primary investigated factors were the cross-sectional vegetative blockage factor (B_X), the distance from the nearest upstream suspended sediment replenishment point, and the flow velocity within floodplain vegetation (u_v).

We used the mean values of B_X and u_v in the regression analysis as the continuous monitoring data showed that deposition occurred at all relative depths (floodplain water depth divided by the total water depth) after vegetation cover had been established. B_X was determined based on 14 overbank flow events for which data could be recorded during the two years, with floodplain water depth ranging at h=0–0.51 m (averaging 0.16 m), relative depth ranging at 0–0.51, and relative submergence (floodplain water depth divided by floodplain vegetation height) ranging at ~0–10. u_v was computed over all four recorded overbank flow events in autumn 2011 (autumn 2010 was so dry that no notable overbank flow events occurred), with floodplain water depth ranging at 0.07–0.51 m and averaging 0.30 m. The SS replenishment point is defined as a sub-reach allowing efficient supply of sediment to the floodplain via lateral advection from the main channel. For the observed mean floodplain water depth of 0.16 m, the computed discharge on the floodplain increased in the sparsely vegetated sub-reaches Bare-M and Willows-M (see Fig. 9), indicating the presence of diverging flows from the main channel in these sub-reaches. A less pronounced increase in discharge was obtained for the sub-reaches Grasses-D and -U at the highest water levels. Supported by visual observations, the sub-reaches Bare-M and Willows-M were considered as SS replenishment points.

The multiple regression analysis was conducted with SPSS Statistics 23 with probability p<0.05 considered as statistically significant. The residuals approximately fulfilled the assumption of homoscedasticity. The residuals were not normally distributed as there were some outliers at both ends. For instance, fairly high net erosion (up to 0.08 m a^{-1}) was recorded in several cross-sections at mid-bank level (see Fig. 3b) while fairly high net deposition (up to 0.15 m a^{-1}) was measured lower on the bank or at the bank toe in the same cross-sections. These high values were expected to be caused by geotechnical erosion while the morphological changes were mostly lower on the floodplain that was merely subjected to hydraulic processes.

4 **Results and discussion**

4.1 Performance of Equation 2 in predicting the drag forces of natural woody plants

Figure 5 shows the performance of Eq. 2 in predicting the drag forces of 0.9–3.1 m tall woody plants of two common species. The measured mean drag force at each examined mean flow velocity (Fig. 5a) was compared to the mean drag predicted by Eq. 2 with the values of χ_F, χ_S, $u_{\chi,F}$, $u_{\chi,S}$, $C_{D\chi,F}$, and $C_{D\chi,S}$ obtained from independent data by Västilä and Järvelä (2014) for the same two species (see Table 2). The mean relative errors were 26% and 14% for the foliated and leafless specimens, respectively (Fig. 5b). The root mean square error and Nash–Sutcliffe efficiency were 1.18 and 0.85, respectively, for foliated specimens, and 0.74 and 0.88, respectively, for leafless specimens. The errors are higher at flow velocities exceeding the range of 0.05–1.0 m s^{-1} recommended for the model (see Jalonen and Järvelä 2014).

The measured data exhibited χ_S= −0.2…−0.47 (as determined with Eq. 1) under leafless conditions and the bulk reconfiguration of χ=−0.58 …−0.83 under foliated conditions at u_m=0.1–1.0 m s^{-1}. Thus, the plants showed notable reconfiguration particularly in the foliated condition, so that the rate of increase in drag with velocity (Fig. 5a) was notably lower compared to the squared rate of increase for rigid cylinders (for which χ=0). The error in χ_S predicted by the model was 0.07−0.15 for each leafless data series while the error in the predicted bulk χ for each foliated data series was 0.02−0.03. Thus, the model (Eq. 2) captured the reconfiguration of the plants reliably, whereas the common assumption of plants being rigid cylinders fails to represent it.

Figure 5 together with the model validation for woody plants with heights of 0.2−0.7 m (Västilä and Järvelä 2014) demonstrate that the same values of the parameters χ_F, χ_S, $u_{\chi,F}$, $u_{\chi,S}$, $C_{D\chi,F}$, and $C_{D\chi,S}$ were able to satisfactorily predict drag forces across a range of over three orders of magnitude (0.05–60 N), with the height of the specimens ranging over one order of magnitude. The apparent size-independency of the model parameters is mainly explained by the separate parameterization of both the foliage and stem, which accommodates the fact that the leaf-area-to-stem-area-ratio and thus the share of the foliage drag to the total drag notable decrease as tree height increases [see e.g. Västilä and Järvelä (2014) and Jalonen and Järvelä (2014) and references therein]. Further, the reconfiguration parameters of the foliage and stem seemed size-independent at the branch and sapling level (Jalonen and Järvelä 2014) although the flexural rigidities of the woody parts of trees generally increase with tree height and age (Niklas 1997; Jalonen and Järvelä 2014).

4.2 Using the proposed parameterization in flow and sediment transport modeling

In this section we demonstrate how the proposed parameterization for woody vegetation (Eqs. 2–6, Figure 6) can be used in hydraulic and morphological models and analyses at plant, plant stand and reach scales. The proposed parameterization is applicable at different levels of relative submergence (h/H) as long as a suitable approach velocity (u_C) is selected (see Fig. 6). The C_Da values can be fed into

3D models (e.g. Lopéz and García 1998; Kang and Choi 2006) or used in analytical models for emergent vegetation (e.g. Vargas-Luna et al. 2015b) while the $C_D aH$ values can be applied when submerged plant stands are analyzed with so-called two-layer approaches (e.g. Luhar et al. 2008; Konings et al. 2012; Luhar and Nepf 2013; Vargas-Luna et al. 2015b). The f'' or n_{veg} values can be used to represent vegetative roughness or vegetative component of the flow resistance in 1–2D models and computations (e.g. McGahey et al. 2008), including HEC-RAS.

With the separate description of the foliage and stem, the parameterization acknowledges the fact that woody plant parts and foliage behave differently under flow. Eqs. 2–6 can therefore be used at different foliation conditions, which allows e.g. estimating the seasonal differences in flow resistance that mainly result from leaf shedding. In addition, the parameterization can also support ecological studies on the effects of erosion and deposition on plant survival (e.g. Pasquale et al. 2014) or on ecosystem engineering by vegetation (e.g. Gurnell 2014). The proposed approach may also be useful for modeling wind flows within tree canopies (e.g. Ayotte et al. 1999; Peltola 2006; Belcher et al. 2012) although further analyses are required to confirm the proper scaling of the parameters for air flows.

Table 2 shows the values of the parameters χ_F, χ_S, $u_{\chi,F}$, $u_{\chi,S}$, $C_{D\chi,F}$, and $C_{D\chi,S}$ for seven common species and four genera of riparian bushes and trees. The values were derived for *Alnus glutinosa*, *Betula pendula*, *Salix alba* × *Salix fragilis*, *Salix viminalis* (the same species that was planted at the present field site), and *Populus nigra* by Västilä and Järvelä (2014), and for *Betula pubescens* and *Salix caprea* by re-analyzing the data of Jalonen and Järvelä (2014). The values were determined by using the same reference velocities ($u_{\chi,F}$=$u_{\chi,S}$=0.2 m s^{-1}) and velocity range (up to u_m=0.8 m s^{-1}) for all species. The inter-specific variation in the parameter values (Table 2) is caused not only by measurement uncertainty and subtle differences in the hydrodynamic behavior between species, but also by slight differences in the research methodology between the two studies. For instance, the lower stem drag coefficients for the species examined by Jalonen and Järvelä (2014) are expected to be largely explained by the usage of the projected one-sided stem area as the reference area as opposed to the frontal projected stem area used by Västilä and Järvelä (2014).

Table 2 includes the species-averaged parameter values computed on the basis of the seven analyzed species. Depending on the species, using the species-averaged instead of the species-specific values causes a mean absolute error of 1−14% (mean: 8%, max: −17%) in the predictions for leafless vegetation and a mean absolute error of 3−30% (mean: 16%, max: 38%) for foliated vegetation assuming A_L/A_S=15 based on Jalonen and Järvelä (2014). The associated errors for foliated vegetation decrease as the share of the foliage drag to the total drag, or A_L/A_S, decreases because the relative inter-specific differences are greater in the foliage drag coefficient ($C_{D\chi,F}$) than the stem drag coefficient ($C_{D\chi,S}$). Overall, it appears feasible to use the species-averaged values in practical applications when riparian areas are populated by a mixture of species. We acknowledge that the parameter values may vary according to e.g. plant size, growth form, or season. Despite these uncertainties, the proposed parameterization provides more accurate and physically-based estimates of the drag of foliated vegetation compared to the commonly made assumption of plants as rigid cylinders.

Figure 7 shows the work flow for estimating vegetative flow resistance using the proposed parameterization. In order to use Eqs. 2–6 for predictive purposes, the values of the parameters need to be known. Depending on the purpose and scale, the foliage and stem reference areas and densities are obtainable e.g. through spectral imaging (e.g. Zou et al. 2009), terrestrial laser scanning (e.g. Jalonen et al. 2015 and references therein; Ma et al. 2016), photographic methods or manual sampling, or literature data (e.g., Tables 2.5 and 3.8 in Zinke 2011; Table 2 in Jalonen et al. 2013). The parameters χ_F, χ_S, $u_{\chi,F}$, $u_{\chi,S}$, $C_{D\chi,F}$, and $C_{D\chi,S}$ representative of a given species can be derived from literature (e.g. Table 2) or from experimental data. Using the values from Table 2, the only additional vegetative properties needed for modeling are the foliage and stem reference areas or densities. The values of the vegetative flow resistance (Eqs. 2–6) need to be solved iteratively since the resistance and velocity are interconnected because of reconfiguration. Finally, resistance values computed through Eqs. 2–6 can be used as direct input to hydraulic and morphological computations and models, replacing the less representative but conventionally applied parameterization of plants as rigid cylindrical elements.

Deriving the values of χ_F, χ_S, $u_{\chi,F}$, $u_{\chi,S}$, $C_{D\chi,F}$, and $C_{D\chi,S}$ experimentally requires either (f'', u_C) data of emergent or just submerged plant stands, or ($\bar{F}$, u_C) data, where $\bar{F}$ denotes the average drag force over several specimens. These data should be obtained at both leafless and foliated conditions at a few relevant values of u_C covering a broad enough velocity range (e.g. $u_C = 0.2-0.8$ m s^{-1}), with velocities of the order of 0.05−0.2 m s^{-1} used as $u_{\chi,F}$ and $u_{\chi,S}$. To ensure accuracy across the whole velocity range it is recommended that $\bar{F}$ data are converted into f'' values through $f''=8\bar{F}/\rho u_C{}^2 A_B$ using the unit bed area ($A_B = 1$ m^2). After determining the associated foliage and stem reference areas, the values of the parameters χ_S and $C_{D\chi,S}$ are obtained by fitting Eq. 2 to the (f'', u_c) dataset of the leafless specimens. The parameters χ_F and $C_{D\chi,F}$ are then derived by fitting Eq. 2 to the (f'', u_c) dataset of the foliated specimens and using the known values of χ_S and $C_{D\chi,S}$. As the parameterization explicitly takes into account the reconfiguration through the terms $(u_C/u_\chi)^\chi$, the drag coefficients and reconfiguration parameters remain constant at the considered velocity range.

4.3 Flow hydraulics and net deposition in the vegetated compound channel

Figure 8 shows the mean velocities within (u_v) and above (u_0) the floodplain vegetation modelled using the two-layer approach (Eqs. 7–8) with C_Da parameterized according to Eq. 3 for the willows. For the modelled flow events, the velocities were notably lower within dense high grasses (u_v=0.02–0.06 m s^{-1}, averaging 0.036 m s^{-1} for sub-reaches Grasses-N, -D, and -U with C_Da=7–24 in autumn 2011) compared to sparser low grasses (mean u_v=0.072 m s^{-1} for Bare-M with C_Da=9) and sparse willows (mean u_v=0.17 m s^{-1} for Willows-M with C_Da=0.06–0.07 above the layer of low grasses). According to the sensitivity analyses, the change of C_D=1 by ±0.5 altered the mean velocities of the grassy sub-reaches by up to few cm s^{-1}: C_D=1.5 resulted in u_v=0.02–0.06 m s^{-1} and C_D=0.5 in u_v=0.03–0.08 m s^{-1}. The modelled discharge on the floodplain increased with increasing floodplain water depth, with the rate of increase notably accelerating after the vegetation became submerged (Figure 9). Thus, the total discharge on the floodplain at the highest water levels was lower for the emergent grassy vegetation (Grasses-N) compared to the submerged vegetation (Grasses-D and -U) for which water flowed mainly above the top of the vegetation with high flow velocities in the unvegetated parts of the cross-section (Fig. 8).

Figure 10 shows the measured mean annual net deposition across the floodplain and bank as derived from the cross-sectional surveys. The factors explaining net deposition are compiled into Table 3. The multiple regression analysis revealed that the net deposition was significantly correlated with the mean cross-sectional vegetative blockage factor (B_X, p<0.001), distance from the suspended sediment replenishment point (x_s, p=0.009), and the estimated mean flow velocity within the vegetation (u_v, p=0.006). The regression explained most of the variation in the observed mean net deposition in the ten cross-sections (adjusted r^2=0.57, Fig. 10), indicating that u_v, B_X, and x_s were the main factors describing the vegetation-induced differences in bulk erosion and deposition. The physical processes captured in the three investigated factors are expected to qualitatively explain the bulk influence of vegetation on net deposition at other sites, as well, (see Section 4.4) although detailed predictions of spatial deposition patterns require considering the turbulent flow structure. Net deposition is also affected by sediment properties, with higher particle settling velocities and incoming sediment loads increasing the rate of deposition (Table 3; e.g. Arboleda et al. 2010).

The particle size distribution of the dispersed, deposited sediment varied depending on the analysis method (Figure 11). Both the hydrometer and laser-based methods resulted in roughly similar share of coarse silt and sand (82 vs 74% finer than 45 µm for Grasses-U and 70 vs 76% finer than 47 µm for Bare-M) but different share of clay (39 vs 11% finer than 2 µm for Grasses-U and 34 vs 12% for Bare-M). The share of the clay fraction is known to be under-estimated by the laser-based method and over-estimated by the settling-based hydrometer method (e.g. Di Stefano et al. 2010). Averaging the results of the two methods, the D_{50} and D_{70} values were 18–32% lower for the dense, high grassy vegetation in Grasses-U (D_{50}=7.4 µm and D_{70}=27) compared to the sparsely vegetated Bare-M (D_{50}=9.1 µm and D_{70}=39).

The computed advection length scales were 16600 m, 990 m and 79 m for the effective floc sizes of 1.3 µm, 7.8 µm and 39 µm (D_{10}, D_{50} and D_{90} of the SS), respectively, with the corresponding settling velocities of 0.15 cm h^{-1}, 2.4 cm h^{-1}, and 31 cm h^{-1}. As an example, the computations showed that 19%, 49% and 92% of the 39 µm flocs were deposited before the flow entered the measured cross-sections in the Grasses-U, -N and -D with the mean distances of 15 m, 39 m and 73 m, respectively, to the SS replenishment point. 5%, 12% and 20% of the total SS load on the floodplain was estimated to be deposited before the flow entered the three sub-reaches. The settling velocities estimated with the relationship of Thonon et al. (2005) for the effective flocculated D_{10}–D_{90} were 1.4–3.5 times higher than those estimated with the Stokes equations for the dispersed D_{10}–D_{90}. The estimated percentages of sediment deposited are directly related to the settling velocity, which highlights the importance of properly considering the flocculation.

4.4 Physical reasoning of the factors explaining the influence of vegetation on net deposition

The present investigation is one of the few studies that experimentally determined how measurable, hydraulically solid properties of natural plant stands control erosion and deposition rates of suspended sediment under real field conditions. The present channel has a low bed slope (0.001) and the estimated flow velocities were fairly low within all floodplain plant stands (Figure 8), and thus the site can be generally classified as a depositional environment. The stream power (Ω) of the 190 m long test reach (based on median annual maximum discharge as estimated from a region-specific empirical nomogram) is approximately 16 W m^{-1}, falling close to the regime characterized by long-term storage of fines within vegetation (Ω<10 W $^{-1}$) as observed in UK rivers by O'Hare (2015).

Net deposition increased with decreasing mean flow velocity within vegetation (Table 3). Thus, the high vegetation densities (C_Da) causing low flow velocities (Figure 8) prevented sediment from being eroded or re-suspended from the floodplain and promoted deposition. The modelled velocities within the vegetation and in the unvegetated part of the cross-section indicated that a vertical shear layer was formed at the top of vegetation when water depth exceeded vegetation height, and another shear layer was formed between the unvegetated main channel and the vegetated floodplain. Although the two-layer model cannot resolve the detailed flow structure in the shear layer, Figure 8 shows that the velocity gradient was stronger for denser vegetation (Grasses-U, -D) compared to sparser, lower vegetation (Bare-M). As schematized in Fig. 2b, the shear layer vortices cannot penetrate to the bottom at high vegetation densities (Nepf 2012), which results in low near-bed turbulence within submerged stands.

The spatially-averaged data revealed that net erosion occurred in the sub-reach Bare-M where the two-year mean spatially-averaged values were ~0.02 m for the vegetation height (H) and 0.19 for the drag–area parameter (C_DaH). By contrast, net deposition occurred in the remaining four sub-reaches with two-year mean C_DaH=0.38–4.9 and H=0.14–0.77 m. These figures were in agreement with the literature value of $C_DaH\approx0.23$ as a density limit between erosion and deposition of suspended sediment (see Fig. 2; Luhar and Nepf (2008)), which supports the applicability of the framework for preliminary estimation of the fate of SS under natural vegetative conditions. In the future, more detailed analyses on the flow structure are needed in particular to determine the lateral transfer of momentum and SS between flexible vegetation and adjacent open water.

Net deposition increased with increasing cross-sectional vegetative blockage factor (B_X, Table 3). The examined compound channel had fairly homogeneous cross-sections, and therefore the vegetative blockage factor was directly related to the height of the floodplain vegetation. In the study of Corenblit et al. (2009) in a gravel-bed river, two-year net erosion and deposition within riparian stands were significantly correlated only with the intercepted biovolume that essentially corresponds to the maximum inundated height for a relatively homogeneous plant cover as in the present case. Thus, the present study strengthens the evidence on the importance of vegetation height, or vegetative blockage at cross-sectional level considerations, in controlling the net deposition within vegetated flows (see also Ganthy et al. 2015). The modeling showed that the discharge passing through vegetation increased with increasing water level until vegetation became submerged (see Fig. 9 where Q_{fp}=Q_v under emergent conditions) and remained fairly constant for higher water levels. Thus, increasing vegetative height (and blockage) enhances the availability of sediment for deposition by increasing the advective supply of SS to the vegetated area (see also Peralta et al. 2008). While the study of Corenblit et al. (2009) considered vegetative parameters corresponding to annual maximum flows, our results indicated that the usage of the annual mean blockage factor was justified for conditions where notable deposition occurred at flow events of different magnitudes.

Net deposition decreased as the distance from the point where sediment is laterally advected onto the floodplain increased (x_s, Table 3), confirming the importance of the longitudinal advective SS supply in controlling the deposition rate. Because of deposition, the availability of SS within vegetation markedly decreases away from the main sediment source since diffusion can supply SS across a limited distance only (e.g. Arboleda et al. 2010; Zong and Nepf 2011). The significant correlation between x_s and net deposition indicated that the lateral diffusion from the main channel and the vertical diffusion from the overflow through shear-layer vortices (see Fig. 2b) could not compensate for the deposition-induced decrease in the sediment load on the inner floodplain. The supply of SS through lateral diffusion was limited mainly to the 1.2 m wide main channel–floodplain interface: for the two sub-reaches located farther away from the SS replenishment point, deposition on the inner floodplain was less than half (on average 0.5 cm a^{-1}) of that on the interface (1.3 cm a^{-1}) despite vegetation height and density differing by less than 20%. The advection length scales indicated that larger flocs rapidly became depleted as water flowed on the floodplain, resulting in finer deposits after a distance of 15 m from the point where the lateral flow of SS from the main channel entered the floodplain (Figure 11). The estimates on the depletion of SS along the floodplain (Section 4.3) were expected to be roughly representative of other small lowland floodplains with similar flow velocities.

Overall, our study showed that net deposition of fines within riparian vegetation is determined by the interplay between sediment supply, effective particle size distribution and the associated settling velocities, and the flow velocity within the vegetation (Table 3). Although deposition has been found to be primarily governed by plant density in small-scale flume studies (Thornton et al. 1997) and in intertidal environments with plant patches (e.g. Bos et al. 2007), not even dense riparian vegetation generates much deposition if there are supply-limited conditions caused by continuous plant stands. On the other hand, if large sediment flocs are supplied, even stands of a relatively low vegetation density (e.g. the present willows with C_DaH=0.38) can promote notable deposition at environments characterized as depositional based on e.g. stream power. The effect of vegetation properties on net deposition is expected to remain qualitatively similar for larger rivers as for the present 10 m wide channel (Table 3). However, quantitative differences are expected because wider floodplains limit the lateral sediment supply more strongly (e.g. Arboleda et al. 2010). In addition, the water depths are higher and the relative submergence of vegetation may be lower for grassed floodplains of larger rivers, which can lead to more efficient vertical supply of SS to the plant stands.

4.5 Implications for sediment management and water quality

Sections 4.3–4.4 show evidence that floodplains inundated at medium to high flows allow managing the transport of fine suspended sediment through suitable maintenance of floodplain vegetation. For instance, vegetative dry mass and height above approximately 200 g m^{-2} and 0.1 m, respectively, were the thresholds for cohesive sediment deposition within natural grasses (Fig. 10; see also Figure 7 in Västilä et al. 2016). Further, the recorded near-bed values of the vegetation density (a) together with the approach of Luhar et al. (2008) summarized in Fig. 2 allow estimating the height of natural grassy vegetation required to prevent erosion. The near-bed a ranged at 6–26 in the five sub-reaches, indicating that a 4 cm high cover of natural grasses would function as erosion protection by exceeding the density limit of C_DaH>0.23 proposed by Luhar et al. (2008). If the flow velocity is high enough to notably bend the grasses so that the drag coefficient decreases to C_D=0.5 in agreement with the sensitivity analysis, a ~10 cm high vegetation cover would be required.

We found that deposition can be supply-limited even on narrow (5 m wide in the present case) vegetated floodplains with estimated settling velocities of as low as $w_s \leq 31$ cm h^{-1} for the effective D_{10}–D_{90}. Further, the results suggested that low levees (longitudinal sediment deposits at the main channel-floodplain interface) can be generated at sites where the suspended sediment is predominantly much finer than typically considered ($w_s \geq 36$ cm h^{-1} in e.g. Sharpe and James 2006; Arboleda et al. 2010; Branß et al. 2016). The formation of levees can have significant implications on the water levels, lateral connectivity and the supply of substances on shallow floodplains. The generation of levees is strengthened by the presence of vegetation (Arboleda et al. 2010) but is also affected by the floodplain water depths: a sub-reach with the maximum relative depth of 0.38 led to ~5 mm/a higher interfacial deposition than that with a maximum relative depth of 0.30 when the effect of vegetation was excluded statistically (see also discussion of Fig. 7 of Västilä et al. 2016). Such differences in the relative depth have been found important in the flume study of Branß et al. (2016), who report that levee width was halved when the relative depth decreased from 0.35 to 0.30.

The low flow channel of the test reach was fairly straight (see Fig. 4), and lateral advection of SS from the main channel took place only at floodplain areas with very low or sparse vegetation. A meandering two-stage channel planform could possibly enhance the supply of SS to the floodplains through flows crossing over from the main channel at bends although dense vegetation may reduce the efficiency of mixing compared to that observed for bare conditions (e.g. Shiono and Muto 1998). Under conditions of inefficient cross-sectional mixing, deposition can be enhanced by ensuring the supply of sediment e.g. through mowing floodplain vegetation from short, regularly-spaced sub-reaches along the channel while maintaining high plant stands elsewhere. By contrast, the supply of sediment, and consequently the deposition on the floodplain, can be reduced by maintaining continuous vegetation strips at the floodplain-main channel interface.

Figure 12 shows the suspended sediment mass balance in the compound test reach. The transported sediment load originated mainly from the catchment, with the fields estimated to have an approximately six times higher specific load than the forested areas (Västilä and Järvelä 2011). Annually, 5.5% of the incoming suspended sediment was deposited on the 190 m long floodplain with the spatially and seasonally averaged vegetation height of 0.25 m (Västilä et al. 2016). 89% of the total suspended sediment load of ~110 t a^{-1} was transported at overbank flows, indicating that the floodplain at the mean water level appeared suitable for enhancing the water quality by trapping sediment. The entire compound reach was fairly homogeneous in vegetation, cross-sectional geometry, sediment load and sediment properties, and therefore we estimated a total annual SS trapping of ~20% on the 850 m long floodplain based on direct up-scaling from the test reach.

The field study demonstrated that constructed floodplains offer potential for controlled deposition and water quality improvements as notable amounts of clay–medium silt are deposited facilitated by the flocculation of the cohesive primary particles (see Figure 11; Middelkoop and Asselman 1998; Thonon et al. 2005; Arboleda et al. 2010). Deposition of the cohesive fraction may reduce the loads of particle-bound phosphorus, pesticides, and heavy metals transported to downstream water bodies. For instance, most of the transported phosphorus is typically sorbed onto fine particles in catchments dominated with cohesive soils (e.g. Uusitalo et al. 2000; Västilä et al. 2015). On the other hand, the accumulation of contaminated sediment on floodplains may affect local ecology and the use of the floodplains for agriculture, or the substances may be released back to the liquid phase through changes in water or soil chemistry. Deposition and vegetation development on excavated floodplains may decrease the conveyance capacity of the channel over time (e.g., Geerling et al. 2008; Villada Arroyave and Crosato 2010), which necessitates vegetation management and periodic lowering of the floodplains. Despite these maintenance requirements, constructed floodplains are an environmentally viable alternative to conventional trapezoidal channels that require frequent, ecologically disturbing dredging of the channel bed (e.g. USDA 2007).

5 Conclusions

Sediment properties are known to be critical for reliable modeling of sediment transport, but the influence of natural vegetation remains less researched. From this starting point we investigated the characterization of natural riparian vegetation for hydraulic and sediment transport analyses by using and amending recently proposed approaches. We combined detailed investigations at the laboratory and field scales, while seeking straightforward practical applicability using physically solid parameterzations. For instance, the field investigations showed that the cross-sectional vegetative blockage factor (B_X) was statistically highly significant in determining the deposition rate for differently vegetated floodplain reaches. In parallel, a parameterization of vegetative drag force (Eq. 2) that incorporates the flexibility-induced reconfiguration was successfully validated for natural woody plants under laboratory conditions. Subsequently, we derived a physically-based parameterization (Eqs. 2–6) for five coefficients and terms that are widely used in hydraulic and morphological modeling to represent the influence of vegetation on flow resistance and structure (summarized in Table 1). The presented parameterization provides a more realistic description of natural vegetation compared to the conventional rigid cylinder approach, allowing reliable estimates under both leafless and foliated conditions. The proposed methodology (Fig. 7) is easy to apply: Eqs. 2–6 (Fig. 6) can be readily implemented into 1D–3D analytical and numerical models using the values of the parameters compiled for common riparian trees and bushes (Table 2). Consequently, the usage of the presented approaches was successfully demonstrated for field-scale analyses.

The field site with cohesive soils and sediment provided new insight into the factors governing net deposition and erosion of fine sediment within natural riparian vegetation. The identified factors (the drag–area parameter C_DaH and the associated flow velocity within vegetation, the cross-sectional vegetative blockage, and the distance from the sediment replenishment point) were shown to capture key processes and were thus expected to apply more broadly to explain the bulk influence of vegetation on deposition. The analyses implied that longitudinal advection was the most important mechanism supplying fine sediment to the floodplain plant stands although continuous stands can limit deposition. From a practical point of view, this study provided guidance on the management of fine sediment by discussing how riparian vegetation can be maintained in order to control erosion and deposition in environmental channel designs. We believe that active vegetation maintenance offers further possibilities, and future studies should be directed towards determining the potential in controlling the fate of pollutants in water courses.

References

Aberle J, Järvelä J (2013) Flow resistance of emergent rigid and flexible vegetation. J Hydraul Res 51(1):33–45. doi:10.1080/00221686.2012.754795

Aberle J, Järvelä J (2015) Hydrodynamics of vegetated channels. In Rowinski P, Radecki-Pawlik A (eds) Rivers – physical, fluvial and environmental processes. GeoPlanet: Earth and Planetary Sciences. Springer, Berlin, pp 519–541. doi:10.1007/978-3-319-17719-9_21

Arboleda AM, Crosato A, Middelkoop H (2010) Reconstructing the early 19th century Waal River by means of a 2D physics-based numerical model. Hydrol Process 24(25): 3661–3675. doi: 10.1002/hyp.7804

Ayotte KW, Finnigan, JJ, Raupach MR (1999) A second-order closure for neutrally stratified vegetative canopy flows. Bound-lay. Meteorol 90:189–216

Belcher SE, Harman IN, Finnigan JJ (2012) The wind in the willows: flows in forest canopies in complex terrain. Annu. Rev. Fluid Mech 44:479–504. doi: 10.1146/annurev-fluid-120710-101036

Bos AR, Bouma TJ, de Kort GLJ, van Katwijk MM (2007) Ecosystem engineering by annual intertidal seagrass beds: Sediment accretion and modification. Estuar Coast Shelf S 74:344–348. doi:10.1016/j.ecss.2007.04.006

Boothroyd RJ, Hardy RJ, Warburton J, Marjoribanks TI (2015) The importance of accurately representing submerged vegetation morphology in the numerical prediction of complex river flow. Earth Surf Process Landforms 41(4): 567–576. doi:10.1002/esp.3871

Branß T, Dittrich A, Núñez-González F (2016) Reproducing natural levee formation in an experimental flume. In Constantinescu G, Garcia M, Hanes D (eds) River Flow 2016. CRC Press, London, pp 1122–1128

Corenblit D, Steiger J, Gurnell AM, Tabacchi E, Roques L (2009) Control of sediment dynamics by vegetation as a key function driving biogeomorphic succession within fluvial corridors. Earth Surf Process Landforms 34(13):1790–1810. doi:10.1002/esp.1876

de Langre E (2008) Effects of wind on plants. Annu Rev Fluid Mech 40:141–168

de Langre E, Gutierrez A, Cossé J (2012) On the scaling of drag reduction by reconfiguration in plants. C. R. Mecanique 340: 35–40. doi:10.1016/j.crme.2011.11.005

Di Stefano C, Ferro V, Mirabile S (2010) Comparison between grain-size analyses using laser diffraction and sedimentation methods. Biosystems Eng 106: 105–115. doi:10.1016/j.biosystemseng.2010.03.013

Dittrich A, Aberle J, Schoneboom T (2012) Drag forces and flow resistance of flexible riparian vegetation. In Rodi W, Uhlmann M (eds) Environmental Fluid Mechanics: Memorial Volume in honour of Prof. Gerhard H. Jirka, IAHR Monographs. CRC Press, London, pp 195–215

Droppo I (2001) Rethinking what constitutes suspended sediment. Hydrol Process 15:1551–1564. doi:10.1002/hyp.228

Fleischer P, Soyeaux R (2013) Technical-biological bank protection on waterways with high traffic frequency – first experience gained from a test stretch at the River Rhine with regard to bank stability. In Rigo P, Wolters M (eds.) Proceedings, 6th International PIANC-Smart Rivers Conference, 23–27 September 2013, Liège, Belgium/Maastricht, the Netherlands. 10 pp

Ganthy F, Soissons L, Sauria PG, Verney R, Sottolichio A (2015) Effects of short flexible seagrass Zostera noltei on flow, erosion and deposition processes determined using flume experiments. Sedimentology 62:997–1023

Geerling GW, Kater E, van den Brink C, Baptist MJ, Ragas AMJ, Smits AJM (2008) Nature rehabilitation by floodplain excavation: The hydraulic effect of 16 years of sedimentation and vegetation succession along the Waal River, NL. Geomorphology 99(1–4):317–328

Gurnell A (2014) Plants as river system engineers. Earth Surf Process Landforms 39:4–25. doi:10.1002/esp.3397

Jalonen J, Järvelä, J (2014) Estimation of drag forces caused by natural woody vegetation of different scales. J Hydrodyn 26:608–623. doi:10.1016/S1001-6058(14)60068-8

Jalonen J, Järvelä J, Aberle J (2013) Leaf area index as vegetation density measure for hydraulic analyses. J Hydraul Eng 139(5):461-469. doi:10.1061/(ASCE)HY.1943-7900.0000700

Jalonen J, Järvelä J, Virtanen J-P, Vaaja M, Kurkela M, Hyyppä H (2015) Determining characteristic vegetation areas by terrestrial laser scanning for floodplain flow modeling. Water 7(2):420-437. doi: 10.3390/w7020420

Järvelä J (2004) Determination of flow resistance caused by non-submerged woody vegetation. Int J River Basin Manag 2(1):61–70

Jeffries R, Darby SE, Sear DA, 2003. The influence of vegetation and organic debris on flood plain sediment dynamics: case study of a loworder stream in the New Forest, England. Geomorphology 51, 61-80.

Kang H, Choi S-U (2006) Turbulence modeling of compound open-channel flows with and without vegetation on the floodplain using the Reynolds stress model. Adv Water Res 29:1650–1664

Kasvi E, Alho P, Lotsari E, Wang Y, Kukko A, Hyyppä H, Hyyppä J (2015) Two-dimensional and three-dimensional computational models in hydrodynamic and morphodynamic reconstructions of a river bend: sensitivity and functionality. Hydrol Process 29:1604–1629. doi: 10.1002/hyp.10277

Konings AG, Katul GG, Thompson SE (2012) A phenomenological model for the flow resistance over submerged vegetation. Water Resour Res 48, W02522. doi:10.1029/2011WR011000

Kouwen N, Fathi-Moghadam M (2000) Friction factors for coniferous trees along rivers. J Hydraul Eng 126:732–740

Li M-H, Eddleman KE (2002) Biotechnical engineering as an alternative to traditional engineering methods: A biotechnical streambank stabilization design approach. Landscape Urban Plan 60:225–242

Li X, Zhang L, Zhang Z (2006) Soil bioengineering and the ecological restoration of riverbanks at the Airport Town, Shanghai, China. Ecol Eng 26:304–314. doi:10.1016/j.ecoleng.2005.10.011

López F, García M (1998) Open-channel flow through simulated vegetation: Suspended sediment transport modeling. Water Resour Res 34(9):2341–2352

Luhar M, Nepf H (2013) From the blade scale to the reach scale: A characterization of aquatic vegetative drag. Adv Water Resour 51:305–316. doi:10.1016/j.advwatres.2012.02.002

Luhar M, Rominger J, Nepf, H (2008) Interaction between flow, transport and vegetation spatial structure. Environ. Fluid Mech. 8:423–439

Ma L, Zheng G, Eitel JUH, Magney TS, Moskal LM (2016) Determining woody-to-total area ratio using terrestrial laser scanning (TLS). Agr Forest Meteorol 228–229:217–228. doi: 10.1016/j.agrformet.2016.06.021

Mahl UH, Tank JL, Roley SS, Davis RT (2015) Two-stage ditch floodplains enhance N-removal capacity and reduce turbidity and dissolved P in agricultural streams. JAWRA 51(4):923–940. doi: 10.1111/1752-1688.12340

Manners R, Wilcox AC, Kui L, Lightbody A, Stella J, Sklar L (2015) When do plants modify fluvial processes? Plant-hydraulic interactions under variable flow and sediment supply rates. Water Resour Res 120(2):325–345. doi:10.1002/2014JF003265

McGahey C, Samuels PG, Knight DW, O'Hare MT (2008) Estimating river flow capacity in practice. J Flood Risk Manage 1(1):23–33

Middelkoop H, Asselman NEM, 1998. Spatial variability of floodplain sedimentation at the event scale in the Rhine-Meuse Delta, the Netherlands. Earth Surface Processes and Landforms 23, 561-573

Naiman RJ, Décamps H (1997) The ecology of interfaces: Riparian zones. Annu Rev Ecol Syst 28:621–658

Nepf H (2012) Flow and transport in regions with aquatic vegetation. Annu Rev Fluid Mech 44:123–142. doi:10.1146/annurev-fluid-120710-101048

Nepf H, Ghisalberti M, White B, Murphy E (2007) Retention time and dispersion associated with submerged aquatic canopies. Water Resour Res 43, W04422, doi:10.1029/2006WR005362

Niklas KJ (1997) Size- and age-dependent variation in the properties of sap- and heartwood in Black Locust (Robinia pseudoacacia L.). Annal Bot 79:473–478

O'Hare M (2015) Aquatic vegetation – a primer for hydrodynamic specialists. J Hydraul Res 53(6):687-698. doi:10.1080/00221686.2015.1090493

Osterkamp WR, Hupp CR, Stoffel M (2012) The interactions between vegetation and erosion: new directions for research at the interface of ecology and geomorphology. Earth Surf Process Landforms 37:23–36. doi:10.1002/esp.2173

Owens PN, Batalla RJ, Collins AJ, Gomez B, Hicks DM, Horowitz AJ, Kondolf GM, Marden M, Page MJ, Peacock DH, Petticrew EL, Salomons W, Trustrum NA (2005) Fine-grained sediment in river systems: environmental significance and management issues. River Res Applic 21:693–717. doi:10.1002/rra.878

Pasquale N, Perona P, Francis R, Burlando P (2014) Above-ground and be-low-ground Salix dynamics in response to river processes. Hydrol Process 28:5189–5203. doi:10.1002/hyp.9993

Peltola HM (2006) Mechanical stability of trees under static loads. Am J Bot 93(10):1501–1511

Peralta G, van Duren LA, Morris EP, Bouma TJ (2008) Consequences of shoot density and stiffness for ecosystem engineering by benthic macrophytes in flow dominated areas: a hydrodynamic flume study. Mar Ecol Prog Ser 368:103–115. doi: 10.3354/meps07574

Powell GE, Ward AD, Mecklenburg DE, Draper J, Word W (2007) Two-stage channel systems: Part 2, case studies. J Soil Water Conserv 62(4):286–296

Schuurman F, Marra WA, Kleinhans MG (2013) Physics-based modeling of large braided sand-bed rivers: Bar pattern formation, dynamics, and sensitivity. J Geophys Res Earth Surf 118:2509–2527. doi:10.1002/2013JF002896

Sellin RHJ, van Beesten DP (2004) Conveyance of a managed vegetated two-stage river channel. Water Management 157(1):21–33. doi:10.1680/wama.2004.157.1.21

Sharpe RG, James CS (2006) Deposition of sediment from suspension in emergent vegetation. Water SA 32(2):211–218

Shields Jr. FD, Coulton KG, Nepf H (2017) Representation of vegetation in two-dimensional hydrodynamic models. J Hydraul Eng, 02517002. doi:10.1061/(ASCE)HY.1943-7900.0001320

Shiono K, Muto Y (1998) Complex flow mechanisms in compound meandering channels with overbank flow. J Fluid Mech 376:221–261

Solari L, van Oorschot M, Belletti B, Hendriks D, Rinaldi M, Vargas-Luna A (2016) Advances on modeling riparian vegetation–hydromorphology interactions. River Res Applic 32:164–178. doi: 10.1002/rra.2910

Studer R, Zeh H (2014) Soil bioengineering - construction type manual. Verein für Ingenieurbiologie, European Federation for Soil Bioengineering. vdf Hochschulverlag AG der ETH Zürich, Switzerland. 440 pp. ISBN 978-3-7281-3642-8. [Open access, http://vdf-online.ch/soil-bioengineering/]

Sukhodolov AN, Sukhodolova TA (2012) Vegetated mixing layer around a finite-size patch of submerged plants: Part 2. Turbulence statistics and structures. Water Resour Res 48:W12506. doi:10.1029/2011WR011805

Thonon I., Roberti JR, Middelkoop H., van der Perk M., Burrough PA (2005) In situ measurements of sediment settling characteristics in floodplains using a LISST-ST. Earth Surf Process Landforms 30: 1327–1343. doi:10.1002/esp.1239

Thornton CI, Abt SR, Clary WP (1997) Vegetation influence on small stream siltation. J Am Water Resour As 33(6):1279–1288

USDA (2007) Two-Stage Channel Design. In National Engineering Handbook, Part 654, Stream Restoration Design. United States Department of Agriculture, Natural Resources Conservation Service

Uusitalo R, Yli-Halla M. Turtola E (2000) Suspended soil as a source of potentially bioavailable phosphorus in surface runoff waters from clay soils. Water Res 34(9):2477–2482

Vargas-Luna A, Crosato A, Calvani G, Uijttewaal WSJ (2015a) Representing plants as rigid cylinders in experiments and models. Adv Water Resourc 93(B):205–222. doi: 10.1016/j.advwatres.2015.10.004

Vargas-Luna A, Crosato A, Uijttewaal WSJ (2015b) Effects of vegetation on flow and sediment transport: comparative analyses and validation of predicting models. Earth Surf Process Landforms 40:157–176. doi:10.1002/esp.3633

Villada Arroyave JA, Crosato A (2010) Effects of river floodplain lowering and vegetation cover. Water Management WM9:457–467. doi: 10.1680/wama.900023

Vogel S (1994) Life in moving fluids – The physical biology of flow, 2nd edition. Princeton University Press, Princeton

Västilä K (2015) Flow–plant–sediment interactions: Vegetative resistance modeling and cohesive sediment processes. Doctoral thesis, Aalto University School of Engineering, Espoo, Finland. http://urn.fi/URN:ISBN:978-952-60-6597-7

Västilä K, Järvelä J (2011) Environmentally preferable two-stage drainage channels: considerations for cohesive sediments and conveyance. Int J River Basin Manage 9(3–4):171–180. doi: 10.1080/15715124.2011.572888

Västilä K, Järvelä J (2014) Modeling the flow resistance of woody vegetation using physically-based properties of the foliage and stem. Water Resour Res 50(1):229–245. doi: 10.1002/2013WR013819

Västilä K, Järvelä J, Aberle J (2013) Characteristic reference areas for estimating flow resistance of natural foliated vegetation. J Hydrol 492:49–60. doi: 10.1016/j.jhydrol.2013.04.015

Västilä K, Järvelä J, Jalonen J (2015) Effect of floodplain vegetation on flow and transport of cohesive particles in an environmental two-stage channel. In Proceedings, 36th IAHR World Congress, 28.6.–3.7.2015, Delft – The Hague, the Netherlands

Västilä K, Järvelä J, Koivusalo H (2016) Flow–vegetation–sediment interaction in a cohesive compound channel. J Hydraul Eng 142(1): 04015034. doi:10.1061/(ASCE)HY.1943-7900.0001058

Whittaker P, Wilson C, Aberle J (2015) An improved Cauchy number approach for predicting the drag and reconfiguration of flexible vegetation. Adv Water Res 83:28–35. doi: 10.1016/j.advwatres.2015.05.005

Wood PJ, Armitage PD (1997) Biological effects of fine sediment in the lotic environment. Environ Manage 21(2):203–217

Xavier P (2009) Floodplain woodland hydrodynamics. Doctoral thesis, Cardiff School of Engineering, Cardiff University, Cardiff, UK

Zinke P (2011) Modelling of flow and levee depositions in a freshwater delta with natural vegetation. Doctoral thesis. Faculty of Civil Engineering, Norwegian University of Science and Technology

Zinke P, Olsen NRB, Bogen J (2011) Three-dimensional numerical modelling of levee depositions in a Scandinavian freshwater delta. Geomorphology 129:320–333. doi:10.1016/j.geomorph.2011.02.027

Zong L, Nepf H (2011) Spatial distribution of deposition within a patch of vegetation. Water Resour Res 47:W03516. doi:10.1029/2010WR009516

Zou J, Yan G, Zhu L, Zhang W (2009) Woody-to-total area ratio determination with a multispectral canopy imager. Tree Physiol 29:1069–1080. doi:10.1093/treephys/tpp042

Table 1 Summary of different formulations used to describe vegetative flow resistance

Formulation	Equation	Common usage
Drag force, F [N]	Eq. 2	F characterizes the drag forces exerted by plants under flow and is commonly applied in experimental investigations
Drag−density parameter, C_Da [m^2 m^{-3}]	Eq. 3	C_Da describes the vegetative drag per unit water volume and is used as a sink or source term in 3D models; closely related to F
Drag−area parameter, C_DaH [m^3 m^{-3}]	Eq. 4	C_DaH is used to characterize the bulk drag of submerged vegetation in approaches that have separate vertical layers for vegetation and overflow; closely related to F
Vegetative friction factor, f'' [-]	Eq. 5	f'' is used to represent the plant-stand scale flow resistance in flume studies and to describe roughness in 2D depth-averaged models
Vegetative Manning coefficient, n_{veg} [-]	Eq. 6	Manning coefficient is widely used to describe reach-scale flow resistance in practical applications and 1D models, or roughness in 2D depth-averaged models

Table 2 Parameter values for the use of Eqs. 2−6 ($u_{\chi,F} = u_{\chi,S} = 0.2$ m s^{-1}). Velocities up to 0.8 m s^{-1} were used in deriving the values

Species	$C_{D\chi,F}$	χ_F	$C_{D\chi,S}$	χ_S	Data source
Alnus glutinosa (Common Alder)	0.18	−1.11	0.89	−0.27	Västilä and Järvelä (2014)
Betula pendula (Silver Birch)	0.20	−1.06	1.02	−0.32	Västilä and Järvelä (2014)
Betula pubescens (White Birch)	0.10	−1.09	0.82	−0.25	Jalonen and Järvelä (2014)
Populus nigra (Black Poplar)	0.13	−0.97	0.95	−0.27	Västilä and Järvelä (2014)
Salix alba × *Salix fragilis* (hybrid Crack Willow)	0.19	−1.21	0.96	−0.25	Västilä and Järvelä (2014)
Salix caprea (Goat Willow)	0.09	−1.09	0.84	−0.27	Jalonen and Järvelä (2014)
Salix viminalis (Common Osier)	0.11	−1.21	1.03	−0.20	Västilä and Järvelä (2014)
Species-averaged	0.14	−1.11	0.93	−0.26	

Table 3. Factors representing vegetation and sediment properties to explain net deposition within floodplain vegetation (statistical significance from the present field data).

Explanatory factor	Effect on net deposition	Statistical significance
Cross-sectional vegetative blockage factor (B_X)	+	Highly significant ***
Flow velocity within vegetation (u_v)	−	Significant **
Distance from sediment supply point (x_s)	−	Significant **
Suspended sediment load	+	Not evaluated/see text
Settling velocity (w_s)	+	Not evaluated/see text

*** $p \leq 0.001$; ** $p \leq 0.01$

Figure captions

Fig 1 Determination of the cross-sectional vegetative blockage factor and interfaces L_b and L_v of Eqs. 7−8

Fig 2 Effect of vegetation on the turbulent flow structure and sediment transport in sparse plant stands (a) and dense plant stands (b), with the density limits (C_DaH) according to Nepf (2012). Patterns #1–#2 relate to turbulence generated by individual plants (#1) and by stand-scale shear layers (#2) [modified from Västilä (2015)]

Fig 3 The field site with the constructed floodplain (a), and a representative cross-section with the measured mean annual net deposition (b)

Fig 4 The test reach with the five differently vegetated sub-reaches, including the locations of main monitoring activities.

Fig 5 Mean drag forces of leafless and foliated, 0.9–3.1 m tall woody plants (Xavier 2009; Jalonen and Järvelä 2014) (a), and mean errors in the drag forces predicted with Equation 2 (b)

Fig 6 Usage of the flow resistance parameterization (Eqs. 2–6) in plant-scale, plant stand-scale, and reach-scale analyses at different relative submergences (h/H). The recommended characteristic approach velocities (u_C) are shown, with u_v denoting the mean velocity in the vegetated part of the cross-section. Equations are written for the drag force (F), vegetative friction factor (f''), drag–density parameter (C_Da), drag–area parameter (C_DaH) and vegetative Manning coefficient (n_{veg}) using the one-sided leaf area (A_L), frontal projected stem area (A_S), unit bed area (A_B), the leaf area per unit volume (a_L) and the stem area per unit volume (a_S). Values of χ_F, χ_S, $C_{D\chi,F}$, $C_{D\chi,S}$, $u_{\chi,F}$, and $u_{\chi,S}$ are reported in Table 2 for common riparian species. Note that all vegetative reference areas refer to the wet parts of the plants

Fig 7 Work-flow for estimating vegetative flow resistance using Eqs. 2–6 (Fig. 6)

Fig 8 The modelled (Eqs. 7−8) bulk mean velocities within and above floodplain vegetation at different flow events. For submerged conditions, the discontinuity at the top of the vegetation (marked with a dashed line) is due to the two-layer representation in Eqs. 7−8.

Fig 9 The modelled (Eqs. 7−8) discharges on the floodplain at different floodplain water depths. The discharge increased more rapidly after vegetation became submerged (as illustrated by the changes in the slopes of the curves for Grasses-U and -D at water depths equaling vegetation height, i.e., ~0.26 m and 0.36 m, respectively). Vegetation in Grasses-N and Willows-M was emergent and in Bare-M fully submerged at all modelled water depths.

Fig 10 Net deposition as measured (mean values for the ten cross-sections with the bars showing ±1 standard error, N=200) and estimated by the multiple regression; also the two-year mean vegetation heights and dry masses are shown. The diagonal line denotes the perfect fit. The explanatory factors of the model were the cross-sectional vegetative blockage factor, distance from the sediment supply point, and the flow velocity within the vegetation.

Fig 11 Particle size distribution of the dispersed, deposited sediment in two sub-reaches determined by laser diffraction and hydrometer methods (bars showing ±1 standard error, N=3–5).

Fig 12 Annual suspended sediment mass balance in the 190 m long compound test reach with the estimated specific loads from fields (40 t km^{-2} a^{-1}) and forests (7 t km^{-2} a^{-1}). Overbank flows conveyed 89% of the incoming sediment load while 5.5% of the total annual load was deposited on the floodplain

Fig1

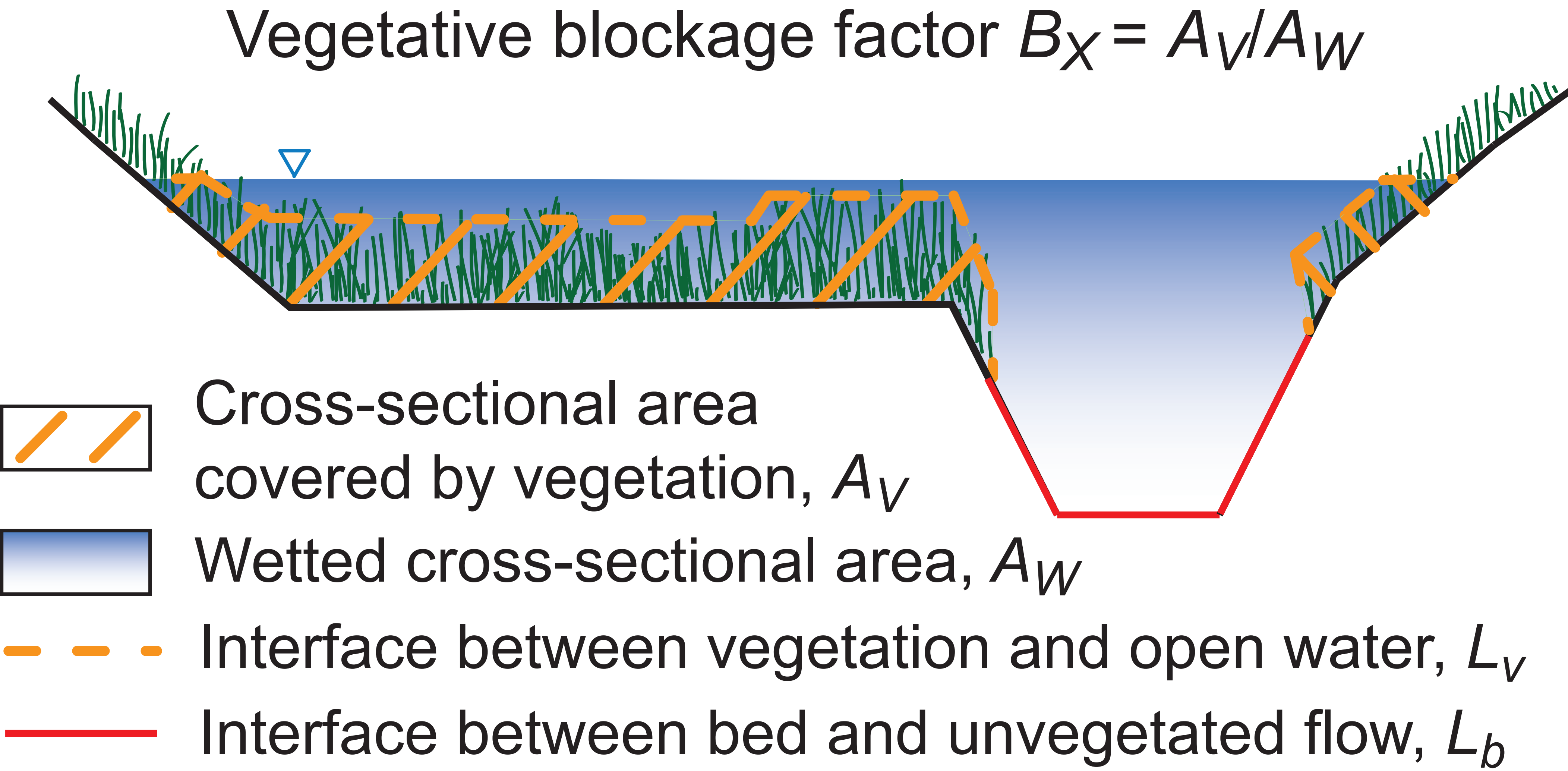

Vegetative blockage factor $B_X = A_V/A_W$
Cross-sectional area covered by vegetation, A_V
Wetted cross-sectional area, A_W
Interface between vegetation and open water, L_v
Interface between bed and unvegetated flow, L_b

Fig2

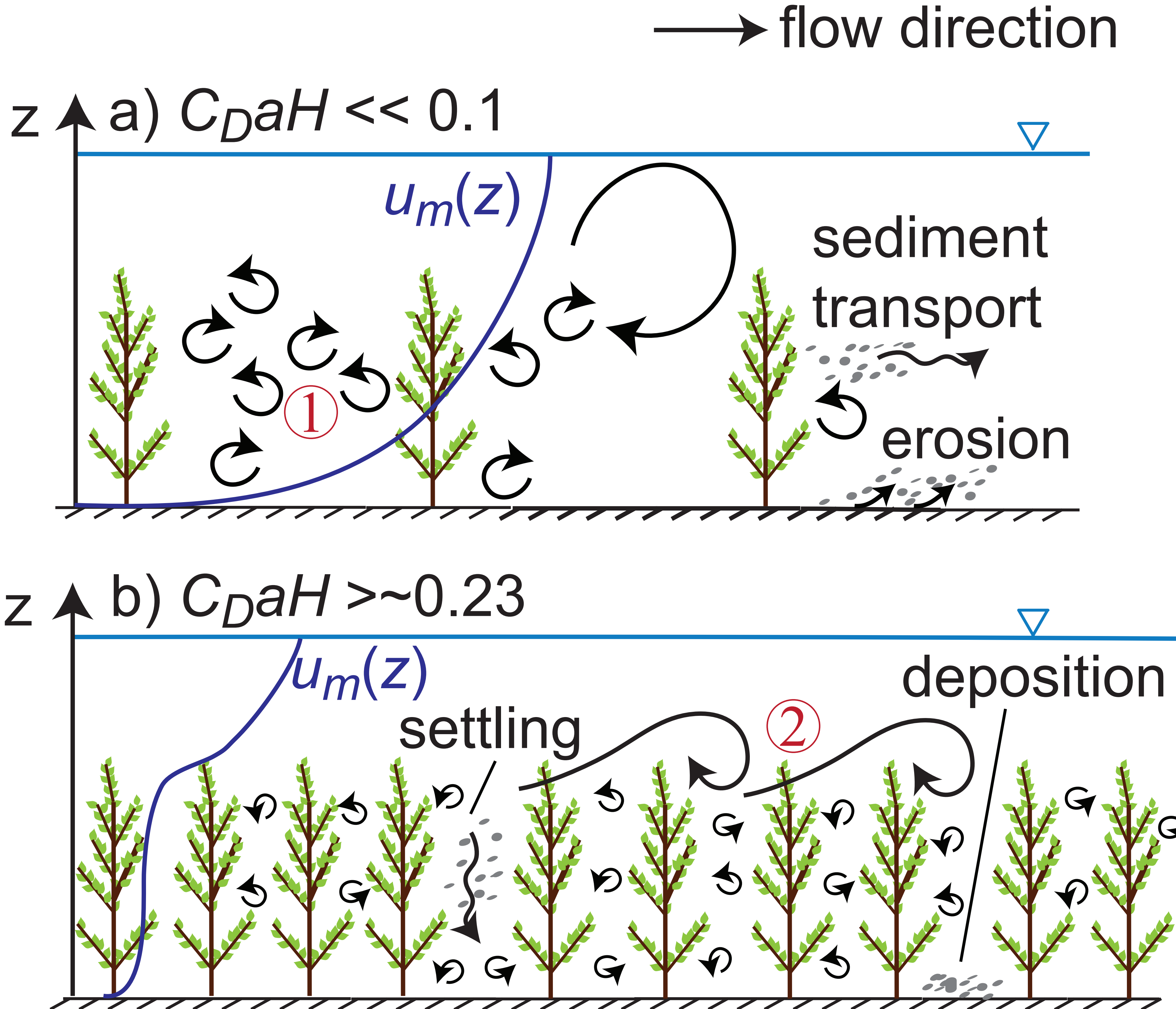

flow direction
a) C_DaH << 0.1
z
$u_m(z)$
sediment
transport
erosion
1
b) C_DaH >~0.23
z
$u_m(z)$
deposition
settling
2

Fig3

a)

b)

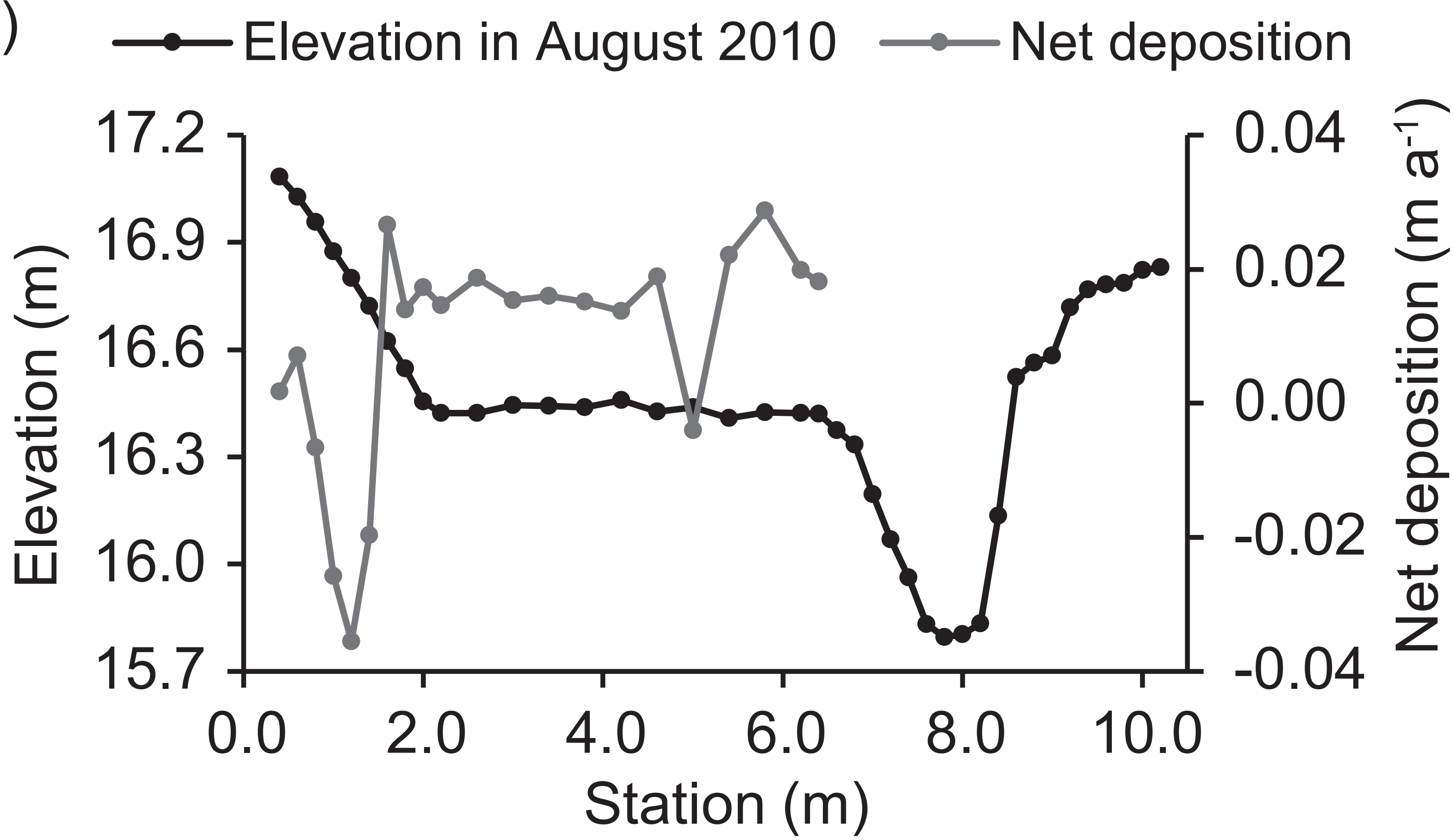
Elevation in August 2010
Net deposition
17.2
16.9
16.6
16.3
16.0
15.7
Elevation (m)
0.04
0.02
0.00
-0.02
-0.04
Net deposition (m a-1)
0.0
2.0
4.0
6.0
8.0
10.0
Station (m)

Fig4

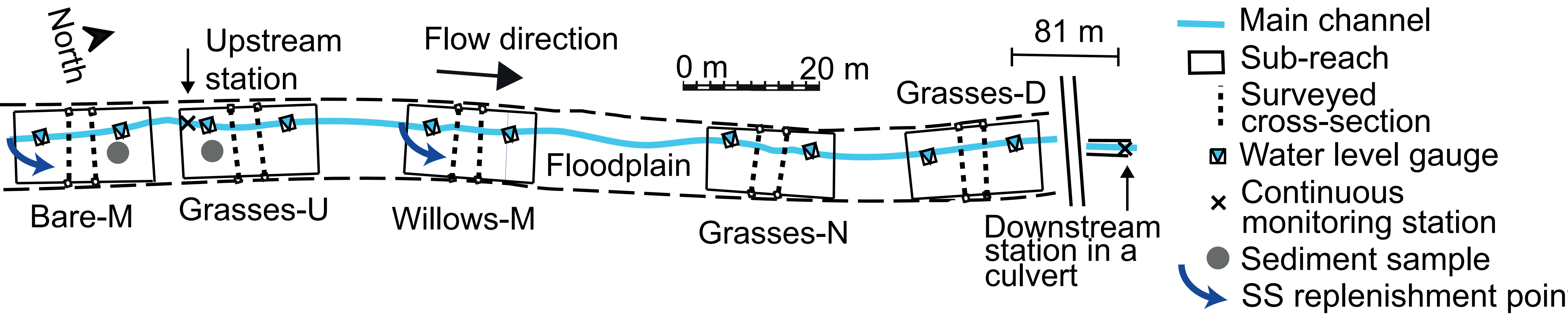

North
Upstream
station
Flow direction
0 m
20 m
81 m
Grasses-D
Floodplain
Bare-M
Grasses-U
Willows-M
Grasses-N
Downstream
station in a
culvert
Main channel
Sub-reach
Surveyed
cross-section
Water level gauge
Continuous
monitoring station
Sediment sample
SS replenishment point

Fig5

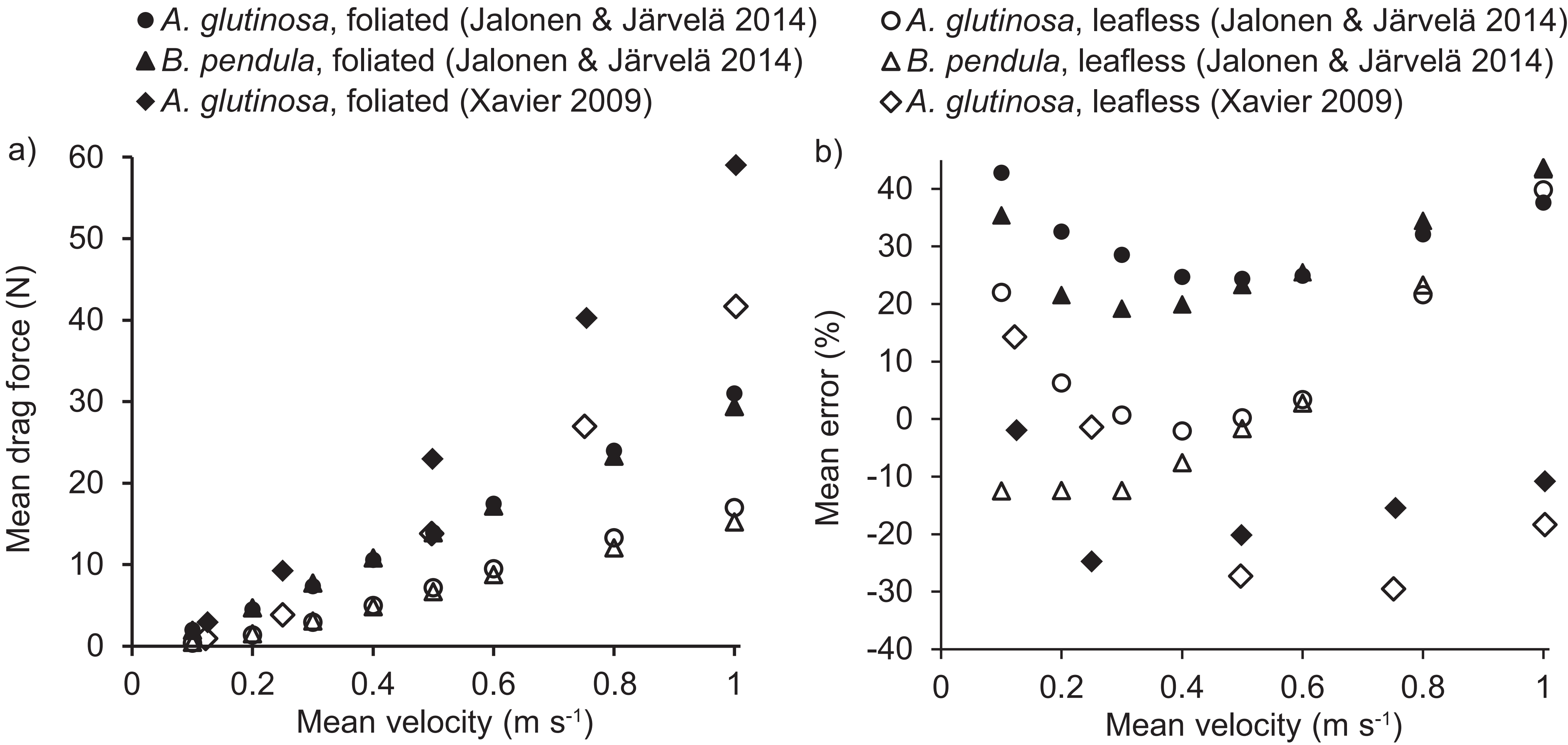

A. glutinosa, foliated (Jalonen & Järvelä 2014)
B. pendula, foliated (Jalonen & Järvelä 2014)
A. glutinosa, foliated (Xavier 2009)
A. glutinosa, leafless (Jalonen & Järvelä 2014)
B. pendula, leafless (Jalonen & Järvelä 2014)
A. glutinosa, leafless (Xavier 2009)
a)
Mean drag force (N)
Mean velocity (m s-1)
b)
Mean error (%)
Mean velocity (m s-1)

Fig6

a) Plant scale

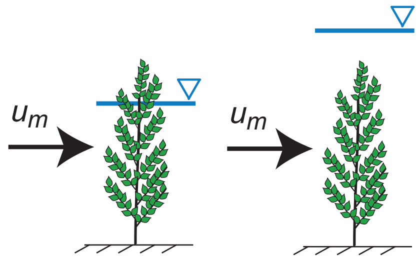

$h/H \leq 1$ $h/H > 1$

For both $h/H \leq 1$ and $h/H > 1$, use depth-averaged mean velocity as u_C with:

$$F = \frac{1}{2}\rho\left[C_{D\chi,F}\left(\frac{u_C}{u_{\chi,F}}\right)^{\chi_F} A_L + C_{D\chi,S}\left(\frac{u_C}{u_{\chi,S}}\right)^{\chi_S} A_S\right]u_C^{\,2} \qquad \text{(Eq. 2)}$$

b) Plant stand scale

(fully developed flow)

$h/H \leq 1$

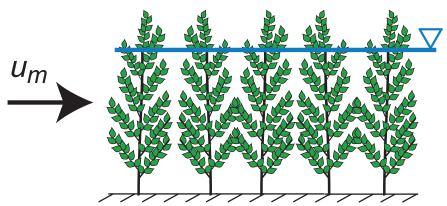

For $h/H \leq 1$, use mean velocity as u_C with:

$$f'' = 4\left[C_{D\chi,F}\left(\frac{u_C}{u_{\chi,F}}\right)^{\chi_F} \frac{A_L}{A_B} + C_{D\chi,S}\left(\frac{u_C}{u_{\chi,S}}\right)^{\chi_S} \frac{A_S}{A_B}\right] \qquad \text{(Eq. 5)}$$

$h/H > 1$

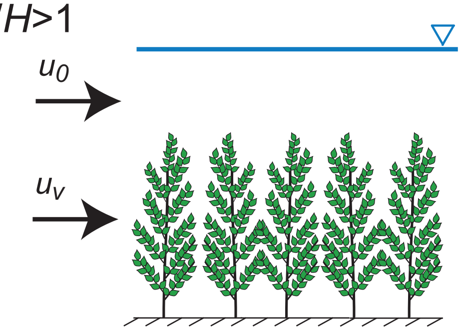

For $h/H > 1$, use $u_C = u_V$ and replace the C_DaH parameter with:

$$C_D a H = C_{D\chi,F}\left(\frac{u_C}{u_{\chi,F}}\right)^{\chi_F} \frac{A_L}{A_B} + C_{D\chi,S}\left(\frac{u_C}{u_{\chi,S}}\right)^{\chi_S} \frac{A_S}{A_B} \qquad \text{(Eq. 4)}$$

c) Reach scale

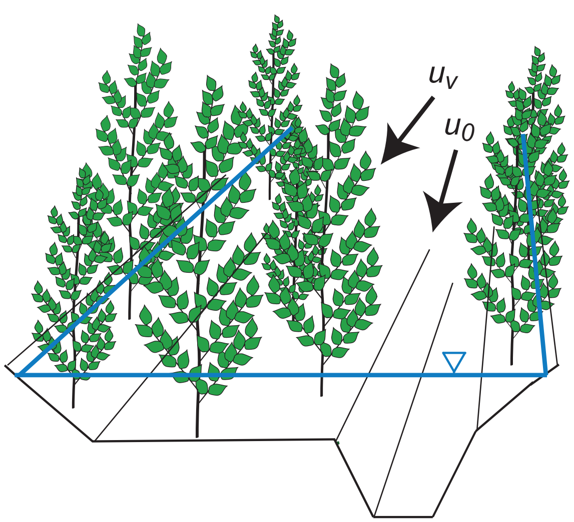

Use $u_C = u_V$ and replace the C_Da parameter in analytical or numerical models with:

$$C_D a = C_{D\chi,F}\left(\frac{u_C}{u_{\chi,F}}\right)^{\chi_F} a_L + C_{D\chi,S}\left(\frac{u_C}{u_{\chi,S}}\right)^{\chi_S} a_S \qquad \text{(Eq. 3)}$$

For practical applications in terms of Manning's n witk K=1 $m^{1/3}$ s^{-1}:

$$n_{veg} = \frac{K h^{1/6}}{\sqrt{2g}}\sqrt{C_{D\chi,F}\left(\frac{u_C}{u_{\chi,F}}\right)^{\chi_F} \frac{A_L}{A_B} + C_{D\chi,S}\left(\frac{u_C}{u_{\chi,S}}\right)^{\chi_S} \frac{A_S}{A_B}} \qquad \text{(Eq. 6)}$$

Fig7

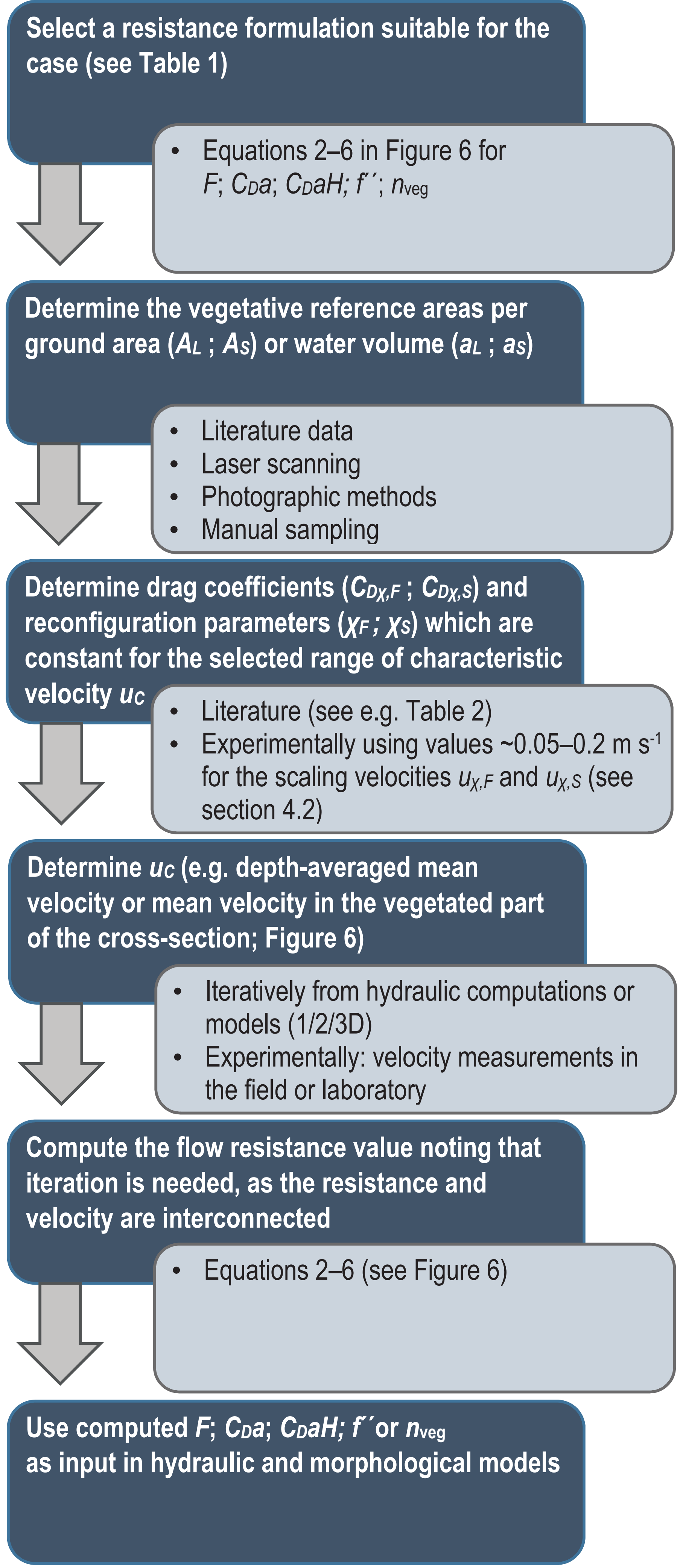
Select a resistance formulation suitable for the case (see Table 1)
• Equations 2–6 in Figure 6 for F; C_Da; C_DaH; f''; n_{veg}
Determine the vegetative reference areas per ground area (A_L ; A_S) or water volume (a_L ; a_S)
• Literature data
• Laser scanning
• Photographic methods
• Manual sampling
Determine drag coefficients ($C_{D\chi,F}$; $C_{D\chi,S}$) and reconfiguration parameters (χ_F ; χ_S) which are constant for the selected range of characteristic velocity u_C
• Literature (see e.g. Table 2)
• Experimentally using values ~0.05–0.2 m s^{-1} for the scaling velocities $u_{\chi,F}$ and $u_{\chi,S}$ (see section 4.2)
Determine u_C (e.g. depth-averaged mean velocity or mean velocity in the vegetated part of the cross-section; Figure 6)
• Iteratively from hydraulic computations or models (1/2/3D)
• Experimentally: velocity measurements in the field or laboratory
Compute the flow resistance value noting that iteration is needed, as the resistance and velocity are interconnected
• Equations 2–6 (see Figure 6)
Use computed F; C_Da; C_DaH; f'' or n_{veg} as input in hydraulic and morphological models

Fig8

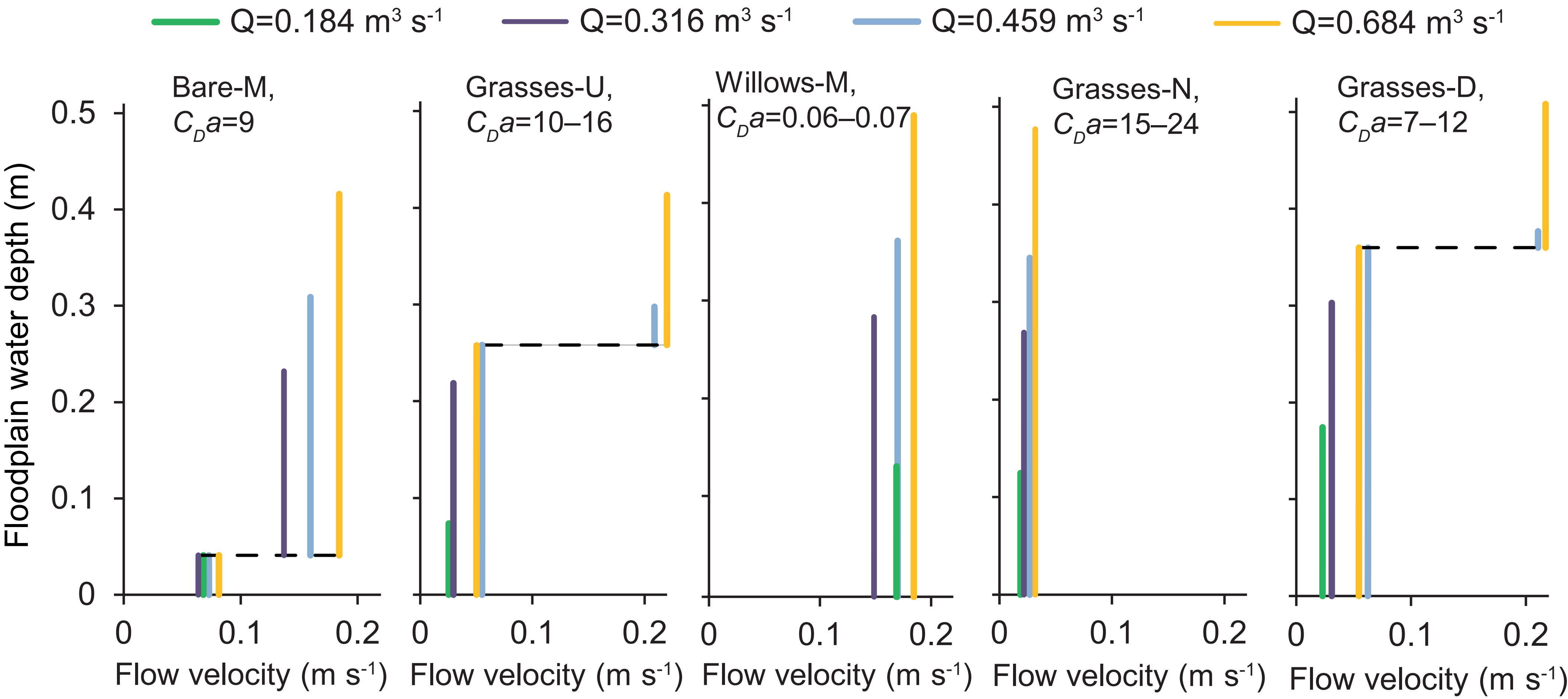

Q=0.184 m3 s-1
Q=0.316 m3 s-1
Q=0.459 m3 s-1
Q=0.684 m3 s-1
Bare-M, CDa=9
Grasses-U, CDa=10–16
Willows-M, CDa=0.06–0.07
Grasses-N, CDa=15–24
Grasses-D, CDa=7–12
Floodplain water depth (m)
0
0.1
0.2
0.3
0.4
0.5
Flow velocity (m s-1)

Fig9

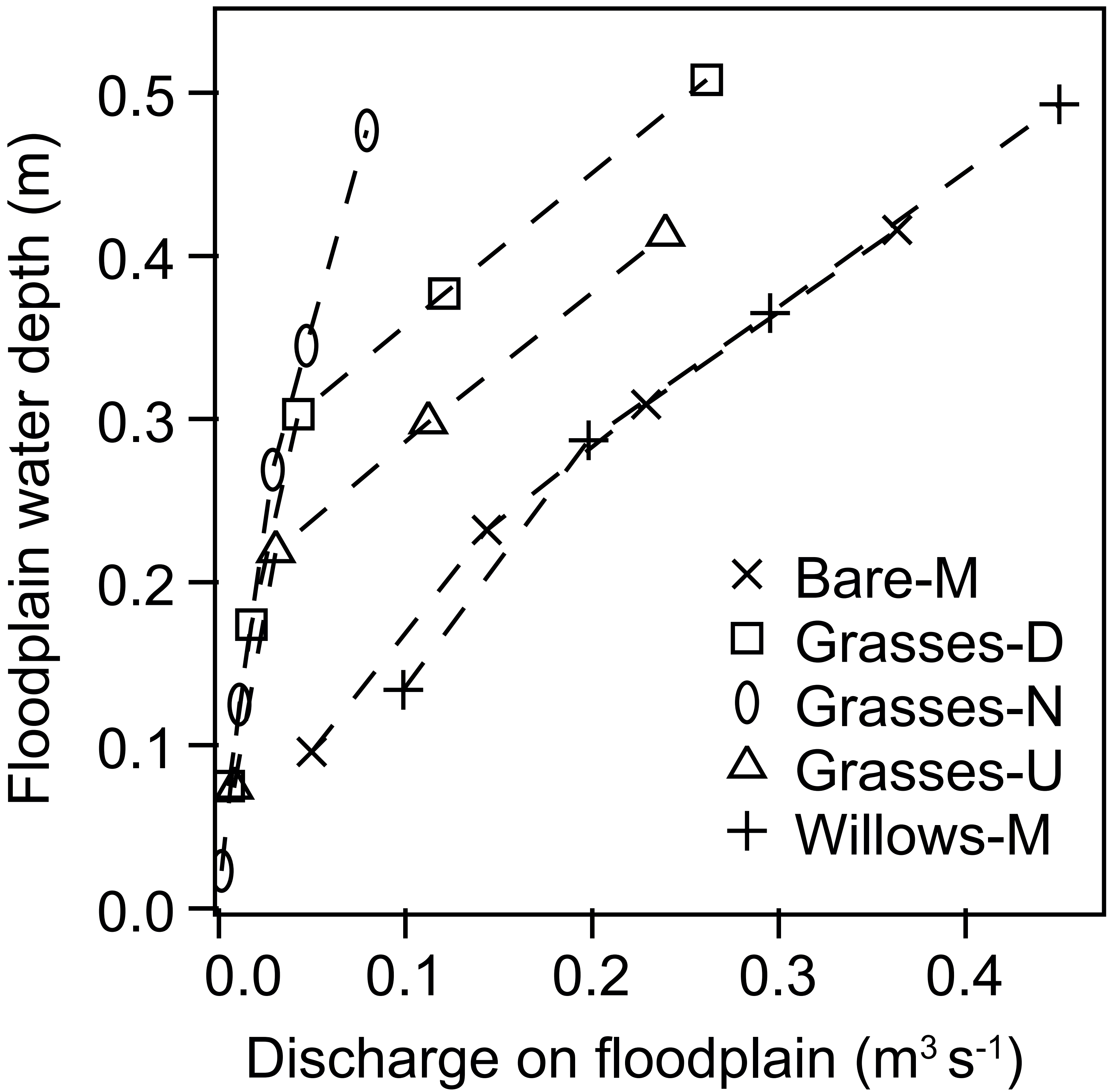

Floodplain water depth (m)
0.0
0.1
0.2
0.3
0.4
0.5
0.0
0.1
0.2
0.3
0.4
Discharge on floodplain ($m^3 s^{-1}$)
Bare-M
Grasses-D
Grasses-N
Grasses-U
Willows-M

Fig10

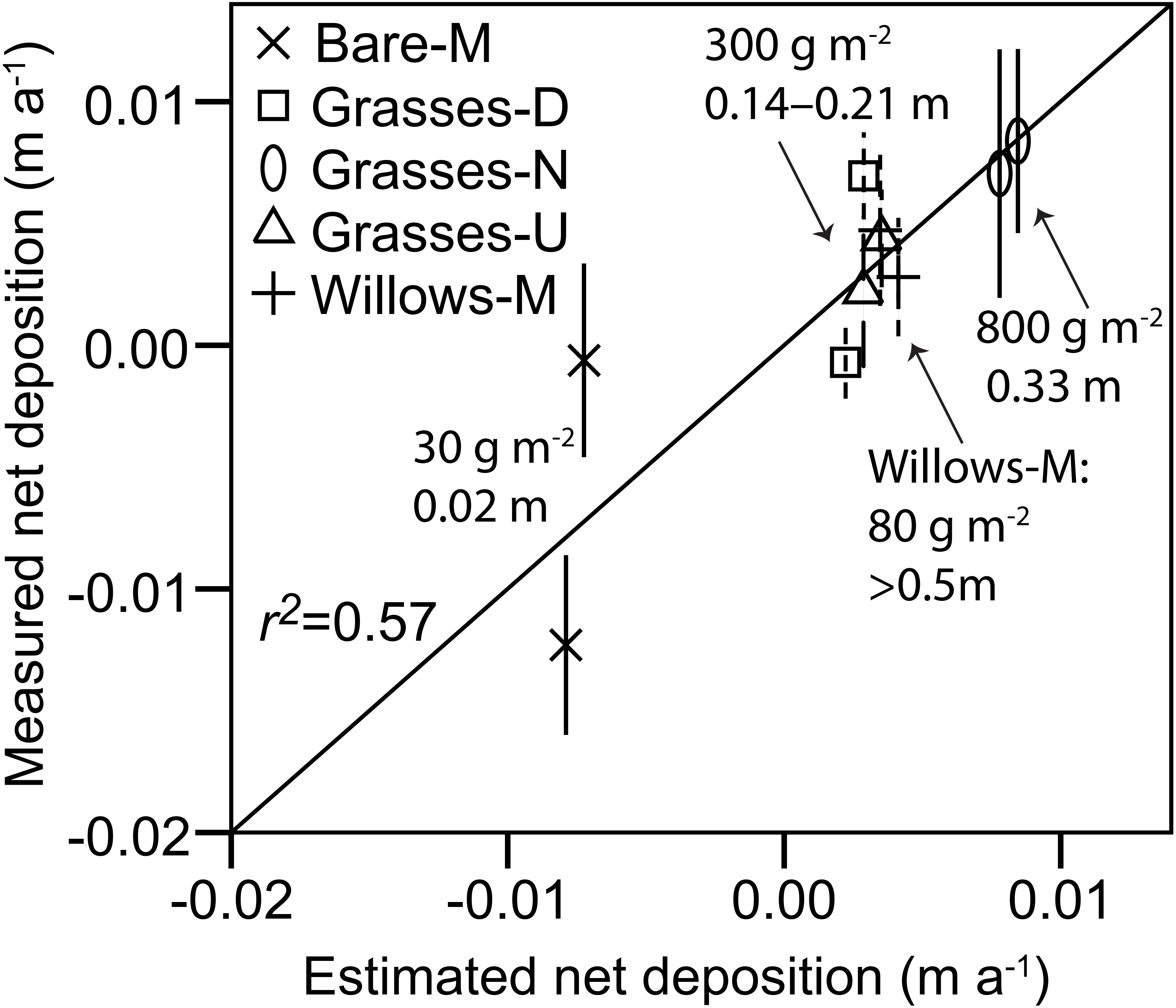

Bare-M
Grasses-D
Grasses-N
Grasses-U
Willows-M
300 g m-2
0.14–0.21 m
800 g m-2
0.33 m
30 g m-2
0.02 m
Willows-M:
80 g m-2
>0.5m
r2=0.57
0.01
0.00
-0.01
-0.02
-0.02
-0.01
0.00
0.01
Measured net deposition (m a-1)
Estimated net deposition (m a-1)

Fig11

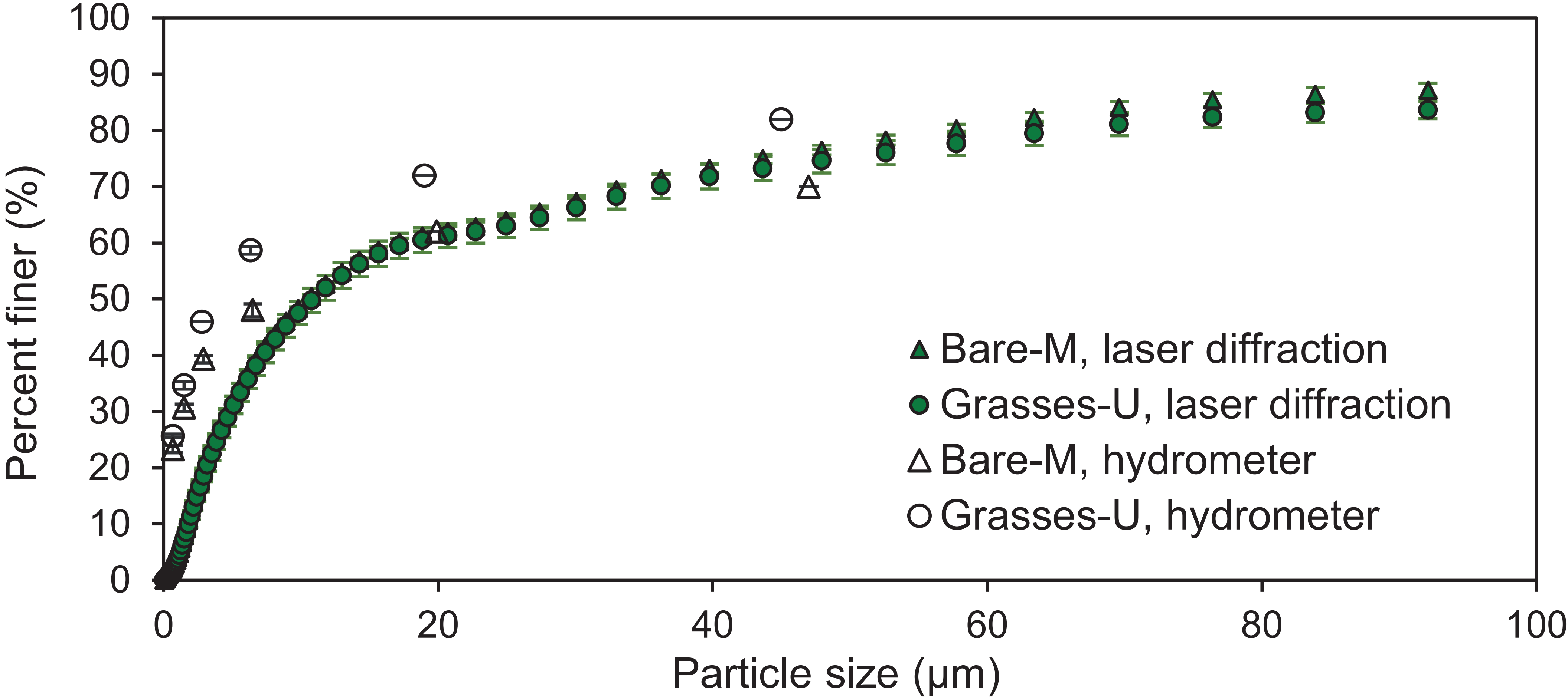

100
90
80
70
60
50
40
30
20
10
0
Percent finer (%)
0
20
40
60
80
100
Particle size (μm)
Bare-M, laser diffraction
Grasses-U, laser diffraction
Bare-M, hydrometer
Grasses-U, hydrometer

Fig12